Invited Research Papers

Groundwater mixing in an alkaline paleolake: Eocene Green River Formation, Wyoming

M'bark Baddouh[a,*], Alan R. Carroll[a], Elliot A. Jagniecki[b], Brian L. Beard[a], Tim K. Lowenstein[c], Clark M. Johnson[a]

[a] *Department of Geoscience, University of Wisconsin, Madison, WI 53706, USA*
[b] *Utah Geological Survey, Salt Lake City, UT, 84114, USA*
[c] *Department of Geological Sciences and Environmental Studies, Binghamton University, Binghamton, NY, 13902, USA*

A B S T R A C T

Tufa in the Little Mesa area of the northern Bridger Basin has been interpreted to record carbonate deposition via subaqueous and subaerial springs emanating near the shoreline of Eocene Lake Gosiute. Sedimentary facies record an overall transgression, culminating with mound structures that reach up to 9 m in height and 40 m in diameter. Mounds exhibit a strong positive, linear covariance between $\delta^{13}C$ and $\delta^{18}O$, defining a slope of ~1. Similar trends occur in many other paleolake deposits, where they are interpreted to reflect changes in evaporation, atmospheric CO_2 exchange, and organic matter burial. However, $\delta^{13}C$ and $\delta^{18}O$ in this study also covary strongly with $^{87}Sr/^{86}Sr$, a new finding that is inconsistent with previously proposed mechanisms. We conclude that Little Mesa isotopic trends reflect mixing of groundwater with low $^{87}Sr/^{86}Sr$, $\delta^{18}O$ and $\delta^{13}C$ and lake water with opposite characteristics. Low $^{87}Sr/^{86}Sr$ in groundwater likely resulted from interaction with marine carbonate strata within the Sevier fold and thrust belt to the west, whereas drainage from Precambrian-cored uplifts that bounded Lake Gosiute to the north, east, and south was responsible for higher lake water ratios.

Little Mesa carbonate facies are all less radiogenic than any time-equivalent facies near the center of the basin, implying horizontal and vertical gradients in Lake Gosiute $^{87}Sr/^{86}Sr$. Previous studies have shown that the lowest $^{87}Sr/^{86}Sr$ in basin center deposits correspond to lake highstands. Results of this study support the hypothesis that climatic modulation of surface runoff and spring emanations from the Sevier belt were principally responsible for precessional-scale expansions and contractions of Lake Gosiute. More broadly, groundwater discharge may represent an important but underappreciated contributor to covariance between $^{87}Sr/^{86}Sr$ ratios, $\delta^{13}C$ and $\delta^{18}O$ in closed paleolake systems.

1. Introduction

Lake deposits have long been recognized for the unique information they can provide on continental tectonics, volcanism, climate, hydrology, and biota. It is well understood that lakes receive water from a variety of sources including direct precipitation on their surfaces, surface runoff from rivers, spillover of upstream lakes, and spring discharge (e.g., Cohen, 2003). The fluxes of water into and out of modern lakes can be directly measured, but reconstruction of the hydrology of paleolakes is more challenging. The magnitude of surface runoff may in some cases be estimated based on channel parameters measured from paleoriver deposits (e.g., Davidson and Hartley, 2010; Trampush et al., 2014) or from the stable isotopic composition of authigenic minerals (e.g., Carroll et al., 2008; Fan and Dettman, 2009; Doebbert et al., 2010). The existence of fill and spill relationships between lakes can also be deduced from the character of preserved facies in adjacent sedimentary basins, provided their relative age relationships are well understood (e.g., Benson and Peterman, 1996; Smith et al., 2008).

Tufa deposits can provide direct evidence of groundwater influx into alkaline paleolakes, based on the inference that such facies record sub-lacustrine spring discharge (e.g., Dunn, 1953; Kempe et al., 1991; Benson, 1994; Smith, 2009). Relief on cylindrical mounds and towers can be locally dramatic, in some cases these structures rise tens of meters above coeval lake floor deposits. The relative importance of spring discharge to the overall hydrology of paleolakes is generally unclear however. Stable isotopic measurements can provide some insight on the mixing of groundwater and lake water (e.g., Benson et al., 1996; Fan et al., 2010) but are also strongly influenced by other factors such as changes in regional precipitation sources, evaporation, temperature, and biological productivity.

Sr isotopes offer an important alternate approach to tracing the provenance of waters responsible for tufa precipitation. Unlike other stable isotopic measures such as $\delta^{13}C$ and $\delta^{18}O$, $^{87}Sr/^{86}Sr$ ratios are not significantly fractionated by meteoric processes or during incorporation into authigenic minerals (c.f. Faure and Powell, 1972; Capo et al., 1998; Doebbert et al., 2014). $^{87}Sr/^{86}Sr$ has been used previously to recognize changes in lake watershed, (e.g., Benson and Peterman, 1996; Gierlowski-Kordesch et al., 2008; Carroll et al., 2008; Doebbert et al.,

---

* Corresponding author.
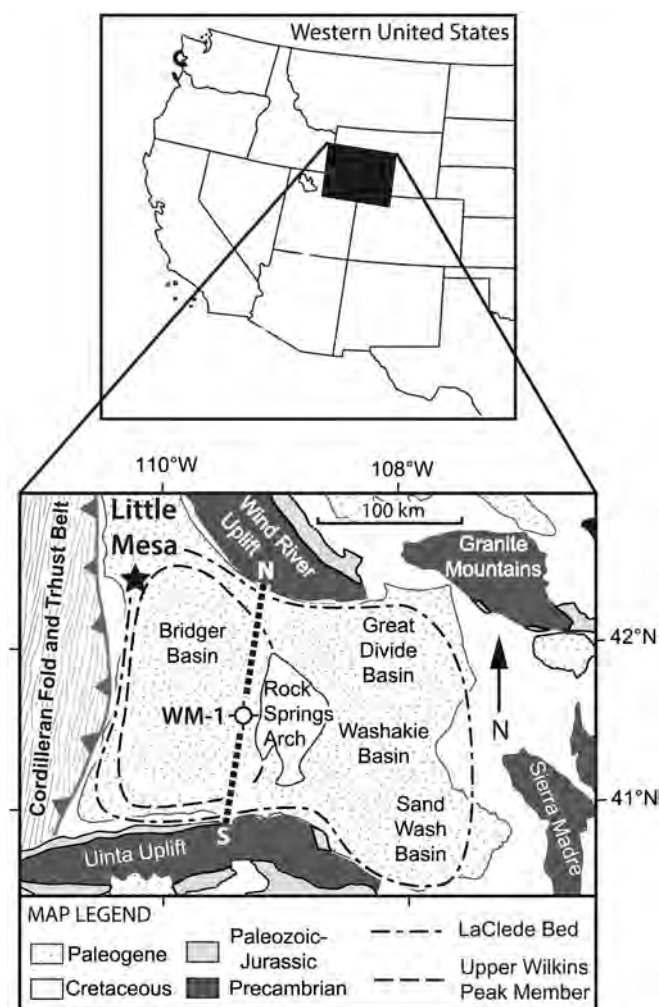 *E-mail address:* mbaddouh@wisc.edu (M. Baddouh).

Fig. 1. Location map. WM-1 = White Mountain # 1 core. N-S cross section shown in figure two. Lateral limits of Wilkins Peak and Laney Members modified from Roehler (1992).

2. Geological setting of the Green River Formation

The Green River Formation in the Bridger Basin includes a wide variety of lacustrine facies associations ranging from fluvial-lacustrine to evaporative (Roehler, 1993; Carroll and Bohacs, 1999; Bohacs et al., 2000). It was deposited in a basin bounded by the Sevier fold and thrust belt to the west and by Laramide-aged basement-cored, reverse-faulted uplifts on the north, south and east (e.g., Dickinson et al., 1988; Fig. 1). The general structural configuration of this region has changed relatively little since the Eocene (cf. Love and Christiansen, 1985).

Previous studies have established large geographic differences in bedrock $^{87}Sr/^{86}Sr$ ratios in areas adjoining the Bridger Basin (Beard and Johnson, 2000; Rhodes et al., 2002; Bataille and Bowen, 2012), which are reflected in the isotopic composition of modern rivers draining from those terrains (Doebbert et al., 2014). To the west of the Bridger Basin, the Cordilleran fold and thrust belt contains structurally-imbricated, Paleozoic-Mesozoic marine carbonate with high Sr concentration, in intervals that may total up to several hundred meters thick. Modern rivers draining this area have $^{87}Sr/^{86}Sr$ ratios of 0.70869 to 0.70917 (Doebbert et al., 2014). In contrast, Laramide uplifts expose more radiogenic Precambrian rocks. Marine carbonate facies generally were eroded from the range crests of these ranges prior to deposition of the GRF (Carroll et al., 2006). Modern rivers that drain these uplifts have reported $^{87}Sr/^{86}Sr$ ratios of 0.7157 to 0.7432 (Doebbert et al., 2014); these higher ratios reflect rocks with high initial ^{87}Rb that has experienced a long period of radioactive decay to ^{87}Sr. The Sr isotopic composition of Green River Formation carbonate appears to mostly reflect variable admixture of waters that drained from the fold and thrust belt versus Laramide uplifts, resulting in $^{87}Sr/^{86}Sr$ ratios mostly in the range of 0.711–0.715 (Doebbert et al., 2014). Less radiogenic volcanic rocks to the north also drained into Lake Gosiute later in its history (Rhodes et al., 2002; Carroll et al., 2008).

Preserved Bridger Basin Green River Formation strata are thickest in the south near the Uinta Mountains, where they exceed 500 m and thin to less than 50 m in the area of Little Mesa (Fig. 2). The Little Mesa mounds are the most prominent feature of a more widespread interval of carbonate facies that spreads ~20 km north-south and extends ~70 km east-west across the northern basin margin (Roehler, 1993; Leggitt and Cushman Jr, 2001). Little Mesa carbonate is laterally equivalent the uppermost Wilkins Peak Member (Fig. 2). Carbonate mounds are also found ~100 km to the southeast of Little Mesa, where they are equivalent to the Tipton Shale Member (Leggitt and Loewen, 2002; Leggitt et al., 2007), and in several other localities.

Little Mesa strata have previously been described by Leggitt and Cushman Jr (2001) and Seard et al. (2013), who concluded that this succession was deposited in nearshore environments by a fluctuating but generally rising lake. The interval described in this study corresponds directly with these previous studies, although details of individual measured sections vary due to lateral facies heterogeneity on the scale of 10s–100s m. Jagniecki et al. (2016) and Lowenstein et al. (2017) proposed that the positions of the mounds were also controlled at least in part by sublacustrine springs, which discharged solutes to the lake. Other large carbonate mound deposits of the Wilkins Peak Member and Laney Member in the southern Bridger and western Sand Wash Basins have likewise been interpreted as a result of Ca^{2+} and HCO_3^--rich spring discharge (Awramik and Buchheim, 2015; Smith et al., 2015).

3. Methods

3.1. Sampling

Two different sample sets were used for this study. Sample set 1, intended to assess temporal trends in carbonate mineralogy and isotope geochemistry, consists of sequential samples from measured sections LM1 and LM2 (lat. 42⁰ 22′ 09″ N, long. 110⁰ 13′ 33″ W) (Fig. 3). Sample

2014), to distinguish between surface runoff vs. groundwater influx (e.g. Neumann and Dreiss, 1995; Hart et al., 2004), and to document periodic changes in basin hydrology paced by precession (e.g., Baddouh et al., 2016, 2017).

The Eocene Green River Formation (GRF) in the Bridger Basin of Wyoming (Fig. 1) is well-suited to examine groundwater influx to paleolakes for several reasons. Deposits of Eocene Lake Gosiute span ~5 My, are generally carbonate-rich, and have been well documented by many detailed stratigraphic, sedimentological, and geochronologic studies conducted over the past ~150 years. An extensive $^{87}Sr/^{86}Sr$ dataset has been published for basin-center deposits (Rhodes et al., 2002; Pietras, 2003; Doebbert et al., 2014; Baddouh et al., 2016, 2017). The GRF also includes carbonate mound deposits, including a ~ 30 m interval exposed at Little Mesa in the Bridger Basin of northwest Wyoming (Fig. 1). The Little Mesa deposits have been previously interpreted as shoreline facies of Eocene Lake Gosiute (e.g., Roehler, 1993; Leggitt and Cushman Jr, 2001; Seard et al., 2013), that may owe their origin to subaqueous and subaerial spring discharge (Jagniecki et al. 2016). In this study we report the first $\delta^{13}C$, $\delta^{18}O$, and $^{87}Sr/^{86}Sr$ data for Little Mesa carbonate facies and examine their relationship to the larger depositional and hydrological evolution of Eocene Lake Gosiute.
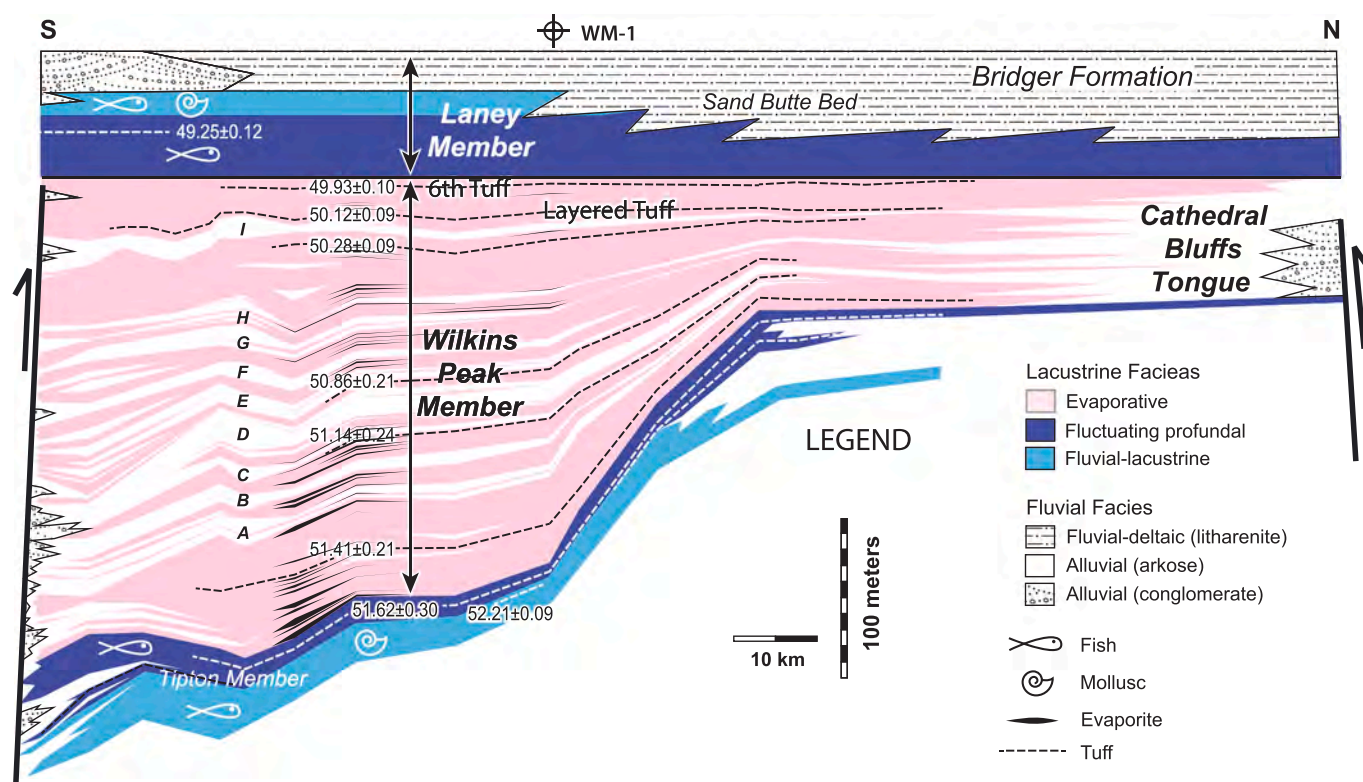
Fig. 2. North South cross-interval across the Greater Green River Basin illustrates the stratigraphic associations between the members of the Green River Formation WM: White Mountain # 1 core. This study focuses on the upper Wilkins Peak Member and lower Laney Member. A through I beds are nine discrete, regionally correlatable intervals of dominantly alluvial, siliclastic lithofacies (Culbertson, 1961; Smoot, 1983). (Modified from Smith et al., 2015). (For interpretation of the references to colour in this figure legend, the reader is referred to the web version of this article.)

set 2 was collected from carbonate mound facies above a distinctive yellow tuff marker bed, identified in this study as the Layered Tuff (Fig. 3; Culbertson, 1961). These samples were collected from the upper ~3–4 m of the Little Mesa carbonate interval in order to assess the range of geochemical variability within the principal mounded horizon. Sample set 2 was not referenced to a specific measured section due to the high degree of lateral facies variation. Boundstone facies from each sample set were sub-sampled by microdrilling ~100 mg from an area ~ 0.5 cm in width and ~ 2 cm in length on polished slabs, avoiding areas of secondary carbonate cement or silica. Four samples from other facies (mudstone, wackestone, and grainstone) were too fine-grained to effectively microdrill specific components, and were instead subjected to crushing and grinding ~100 g of rock with a mortar and pestle.

3.2. Tuff major-element oxides

Electron probe microanalysis of biotite phenocrysts was used to help identify a distinctive yellow marker tuff that occurs within the Little Mesa section, via geochemical comparison to tuffs that occur within the upper Wilkins Peak Member near the basin center (Culbertson, 1961; Smith et al., 2003, 2008, 2010; Machlus et al., 2015). Its most likely correlation is either to the Layered Tuff, which occurs ~24 m below the Wilkins Peak/Laney Member contact in the White Mountain-1core (Figs.1, 2), or the Sixth Tuff, which occurs ~4 m below the contact (Fig. 2).

Major oxide concentrations were measured on 9 biotite grains separated from the Little Mesa marker tuff (15 analyses), and on 23 biotite grains from the Layered Tuff (n = 116 analysis). EPMA wavelength-dispersive spectrometer (WDS) measurements were made at 15 keV, using a 6 nA, 4 μm defocused beam, with 10 s peak and 10 s background counting times, and F Ka with TAP and O Ka with 60 Å LDE

on a Cameca SX51 instrument. These conditions are analogous to those used by Smith et al. (2006), who published analyses of biotite phenocrysts in the 6th Tuff (2 grains, n = 74 analysis).

3.3. Mineralogy

Thin sections of the Little Mesa carbonate were stained with Alizarin red S to differentiate between calcite and dolomite (calcite stained pink/red). Also, petrographic microscopy was used to identify mineralogy and make PPL and XPL photos. X-ray diffraction (XRD) was used to determine bulk mineralogy of carbonate. Powdered samples were put on glass sample holders and analyzed in the Rigaku Rapid II diffractometer with a curved two-dimensional imaging plate that is housed in the University of Wisconsin-Madison. A Mo Ka X-ray tube was used and operated at 50 kV and 50 mA (rated at 2.5 KW). Combination of the 2D imaging plate and the high intensity X-ray source gives increased diffraction X-ray intensity. The MDI DataScan4 and JADE software were used for phase identification and quantitative analysis. JADE software allows the user to identify the peak of each mineral based on its 2θ angle and d value by using multiple databases that provide information about each mineral. After identifying each phase, the software quantifies the percentage of each mineral in each sample.

3.4. Stable isotopes

Powdered splits of sample sets 1 and 2 were placed in glass tubes and shipped for oxygen and carbon isotopes analysis at the Keck Paleoenvironmental & Environmental Stable Isotope Laboratory, Kansas University. About 100 to 200 μg of carbonate samples and standards were weighed in Exetainer tubes and then treated with helium for 5 min. Standards were run at the beginning and end of the
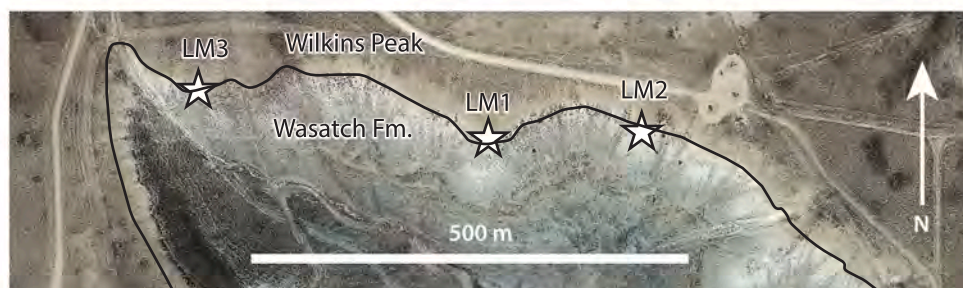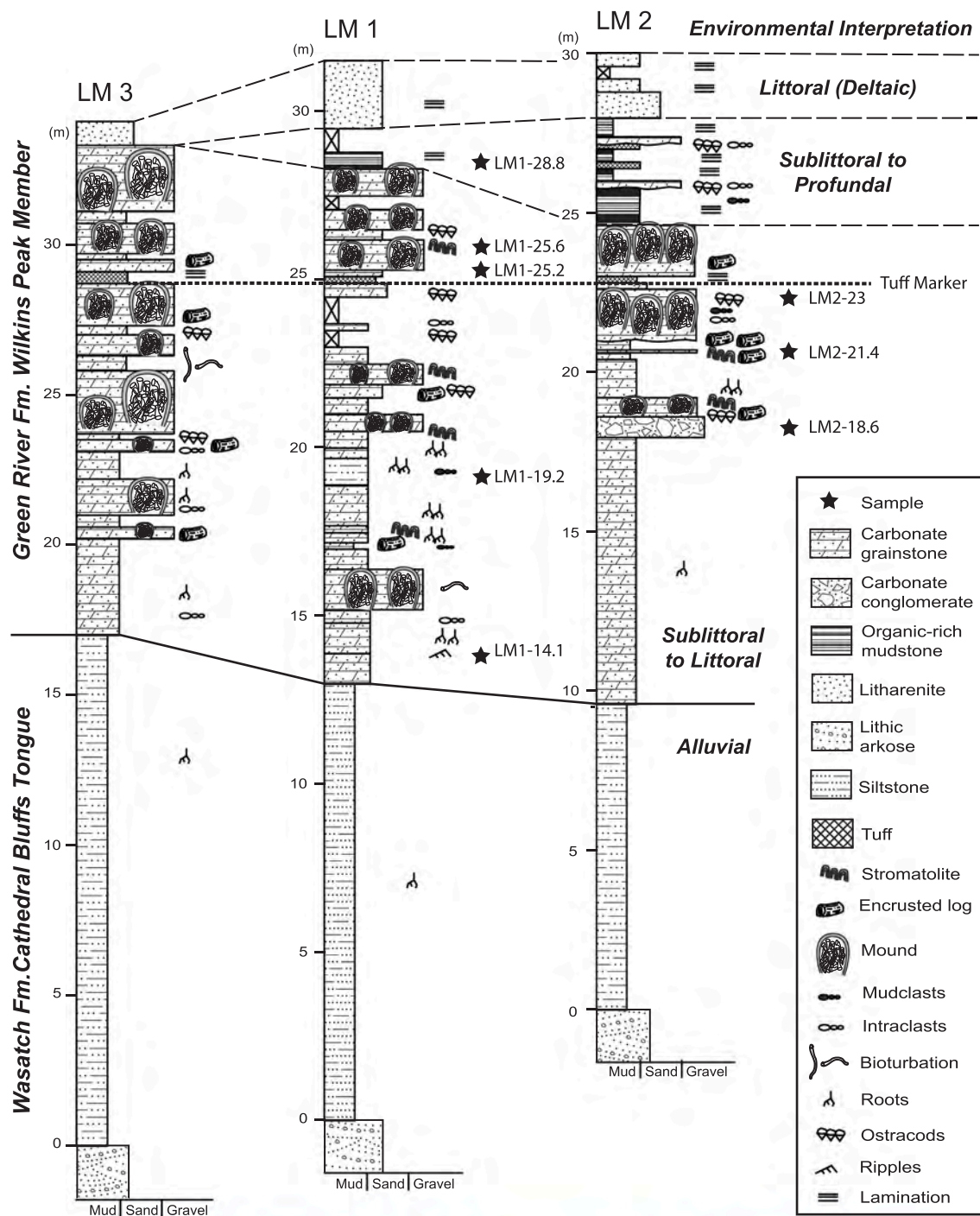
Fig. 3. Stratigraphic sections measured in the Little Mesa (LM) area. Green and red hues on satellite photo correspond to Cathedral Bluffs Member alluvial facies; white to tan hues are lacustrine carbonate facies. LM 1 located at 42.37245°N, 110.21901°W, LM 2 at 42.37247°N, 110.21690°W, and LM 3 at 42.37322°N, 110.22297°W (WGS84 datum). (For interpretation of the references to colour in this figure legend, the reader is referred to the web version of this article.)

sample queue, and after each set of 10 samples. A four-point calibration curve was generated using four standards: NIST NBS-18 ($\delta^{13}C = -5.01$, $\delta^{18}O = -23.20‰$, VPDB), NBS-19 ($\delta^{13}C = 1.95$, $\delta^{18}O = -2.20‰$, VPDB), internal standard Calcite-1 ($\delta^{13}C = -6.05$, $\delta^{18}O = -3.67‰$, VPDB), and internal standard Merck Calcium Carbonate ($\delta^{13}C = -35.58$, $\delta^{18}O = -16.33‰$, VPDB). The calibration curve typically yielded $R^2 = 0.9995$). The precision is better than 0.06‰ for carbon and 0.12‰ for oxygen.

Approximately 3 to 4 drops of 100% phosphoric acid was added and allowed to dissolve the carbonate for 24 h at 25 °C to release CO_2. Analysis was performed using ThermoFinnigan GasBench II in line with Finnigan MAT 253 isotopes ratio mass spectrometer. The Isodat software analyzed 5 sample peaks per sample, using only the average of the last 4 per chromatogram to determine $\delta^{13}C$ and $\delta^{18}O$.

3.5. Radiogenic isotopes

Carbonate Sr isotope ratios, Rb and Sr concentrations, and percent carbonate were measured from 5 mg to 100 mg powdered aliquots of Sample Sets 1 and 2. All samples were dissolved in 8 M HCl, then spiked with a mixed $^{87}Rb-^{84}Sr$ tracer to determine Rb and Sr concentrations by isotope dilution mass spectrometry (IDMS). $^{87}Sr/^{86}Sr$ ratios were analyzed using a VG Instruments Sector 54 multi collector thermal ionization mass spectrometer. The reported $^{87}Sr/^{86}Sr$ ratio is based on the average of 120 ratios with an ^{88}Sr ion intensity of 3×10^{-11} A. Reported errors are the internal 2-standard errors (2-SE), which is slightly less than the long-term external error. The latter is defined as 2 standard deviations of the mean based on the NIST SRM-987 Sr isotope standard, which resulted in values of 0.710264 ± 0.000016 (2σ, $n = 32$) and 0.710262 ± 0.000016 (2σ, $n = 66$) during analysis of sample sets 1 and 2, respectively. See Doebbert et al. (2014) for a more detailed description of analytical methods.

4. Results

4.1. Tuff marker bed identification

The physical characteristics of the Little Mesa yellow marker tuff are consistent with it being an upwind equivalent of the Layered Tuff of Culbertson (1961). Both contain a similar distinctive pattern of internal lamination (Fig. 4) that does not occur in other major tuffs. Geochemical analysis of trace elements in biotite phenocrysts in the Little Mesa yellow marker tuff also more closely match those in the Layered Tuff than the Sixth Tuff (Table 1; Fig. 5). The Little Mesa marker tuff is about twice as thick as the Layered Tuff at city of Green River.
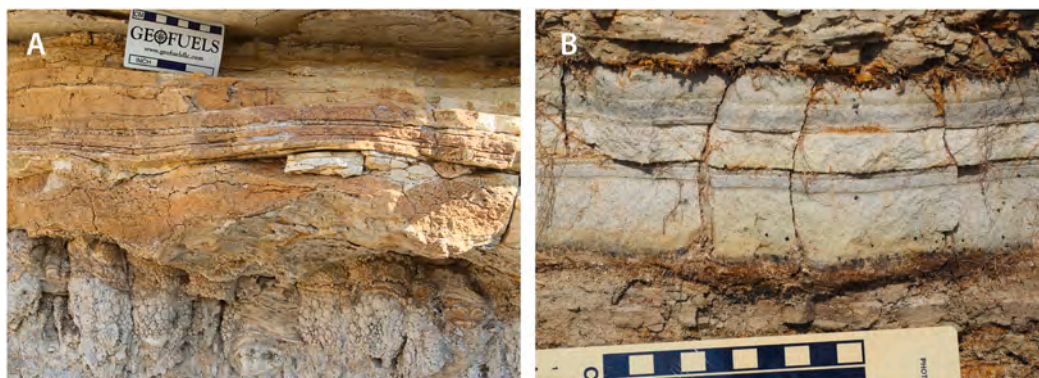
Table 1
Summary of major oxide analyses of tuff biotite phenocrysts.

Oxide	Little Mesa tuff ($n = 15$)		Layered tuff ($n = 115$)		Sixth tuff (n-74)	
	Weight percent	SE	Weight percent	SE	Weight percent	SE
SiO_2	33.15	0.40	33.35	0.40	34.80	0.47
TiO_2	4.02	0.31	3.86	0.30	5.10	0.22
Al_2O_3	14.45	0.27	14.49	0.27	14.00	0.31
FeO	24.80	0.48	24.76	0.49	20.50	0.66
MnO	BDL	N/A	BDL	N/A	BDL	N/A
MgO	6.36	0.15	7.19	0.16	10.30	0.26
CaO	BDL	N/A	BDL	N/A	BDL	N/A
Na_2O	0.35	0.04	0.49	0.06	0.50	0.09
K_2O	7.81	0.17	8.03	0.17	8.33	0.25
BaO	0.76	0.07	0.78	0.08	1.16	0.46
F	BDL	N/A	BDL	N/A	BDL	N/A
Excess O	7.03	0.08	5.58	0.07	3.55	0.04
Total	99.20		99.16		100.40	

1. EPMA WDS measurements made at 15 keV, using a 6 nA, 4 μm defocused beam, with 10 s peak and 10 s bkg. Counting times, and F Ka with TAP and O Ka with 60 Å LDE on a Cameca SX51 instrument.
2. Analyses made on transects orthogonal to the c-axes of 9 biotite grains from Little Mesa tuff and 23 biotite grains fro Layered tuff (this study), and two biotite grans from the 6th tuff (Smith et al., 2006).
3. Excess O is unaccounted for in stoichiometric apportionments, and likely represents conversion of Fe2 + to Fe3 + or addition of OH/H2O.
4. BDL-below detection limit. 4.
5. N/A = not applicable.
6. SE = Standard Error.

4.2. Sedimentary facies

The carbonate interval at Little Mesa is underlain by siliciclastic mudstone to sandstone deposits of the Cathedral Bluffs Member of the Wasatch Formation, which are laterally equivalent to the Green River Formation downdip (Roehler, 1992). The Cathedral Bluffs Member contains little carbonate, aside from nodules associated with paleosol horizons. The contact with the carbonate interval generally appears gradational, but it is relatively poorly exposed and local scour of up to 1–2 m cannot be excluded. Siliciclastic grains appear to have been reworked into the lowermost carbonate-bearing sample in this study (LM1–14.10-2; Fig. 6a), which contains ~40% quartz and feldspar and ~ 7% illite (Table 2).

The carbonate interval grades upward from grainstone at its base, to boundstone mounds at the top. The grainstone appears to consist primarily of sand-size intraclasts, although precise grain sizes are difficult to determine due to carbonate cementation. It also includes fragments of mound facies. Shingled, low–relief bedforms are visible near the base

Fig. 4. Outcrop photos comparing the Layered Tuff in city of Green River to the Little Mesa Tuff Marker bed. Note similarity of internal layering at each locality and difference in scale (tuff bed is thicker at Little Mesa). (For interpretation of the references to colour in this figure legend, the reader is referred to the web version of this article.)
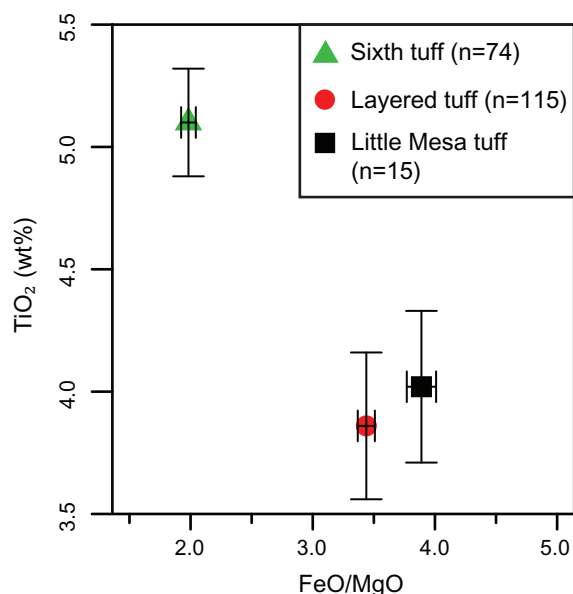
Fig. 5. Cross-plot of TiO_2 vs. FeO/MgO weight percent of biotite grains from Little Mesa Tuff Marker, Layered and Sixth Tuffs.

of this interval, and trough cross-beds are preserved in some grainstone facies farther up-section. Isolated mounds and stromatolite horizons increase in frequency up-section. Sub-horizonal, cylindrical structures, interpreted to represent downed tree trunks and branches that have been encrusted by stromatolite, are dispersed in the middle to upper part of the carbonate interval (Leggitt and Cushman, 2001; Seard et al., 2013). These occur both as isolated structures ~10 cm −1 m in diameter, and in groups arranged approximately parallel to each other and to bedding. Stromatolite coatings are often asymmetric, with thicker laminae on one side. No structures suggestive of stumps or roots were observed.

The largest and most closely-spaced mounds are concentrated near the top of the carbonate interval. They have commonly been broken or toppled, then re-coated with stromatolite facies. Mound buildups at the study location form circular shapes up to 1 m in diameter and up to 2 m in height (Leggitt and Cushman Jr, 2001). The cores of the mounds typically consist of amalgamated tube-shaped structures ~1 cm long and ~ 2.5 mm in diameter, that have been interpreted previously to be mineralized caddisfly larval cases (Fig. 6b, c; Leggitt and Cushman Jr, 2001). Sub-parallel tubes typically clump together in groups, which display a variety of different orientations. The centers of the tubes may be either empty or filled with dark dolomicrite peloids or megaquartz cement (Fig. 6b, c). Chert, chalcedony, ostracods, and ~ 100 μm, light-colored spheres of uncertain origin are also represented in these samples (Fig. 6b–d and 7a–d).

A typical tube's internal structure starts with a 50 μm laminated section which is interpreted to be dolomite because it does not stain pink from Alizarin red S. The next layer is about 300 μm calcitic (stained pink) layer with wavy shape. Finally, thicker dolomicrite layer with fine dark green matrix with well-organized peloids and less commonly ostracods in the outer layer. Tubes are attached to each other by calcite cement or dark green micrite to dolomicrite matrix forming intragrain spaces that are filled with detrital material such as peloids, ostracods, as well as megaquartz, chert, and chalcedony cements (Fig. 6b and c).

Little Mesa stromatolite consist of alternating calcite, dolomite, and dark organic-rich lamina directly encrusting tubes, logs and dolomicrite peloids (Fig. 8a). Concentric stromatolite layers build up to form domes and continuous planar layers, sometimes exceeding 1 m in aggregate thickness. Partial to complete silicification is common (Fig. 8b). Laminae are thin (~100 μm) and continuous (Fig. 8a). At the cm scale,

stromatolite commonly forms digitate morphologies, that internally consist of rows of ~100 μm spherical structures alternating with ~100 μm laminae of darker-colored micrite (Fig. 8b). The spheres have variously been interpreted as green algae fungal spores, or insect eggs (e.g., Bradley, 1929; Leggitt and Cushman Jr, 2001; Seard et al., 2013)

Inter-mound spaces are filled with peloids, ostracods, and calcimicrite to dolomicrite intraclasts (Fig. 7d). Peloids are rounded, dark green dolomicrite with different sizes (100–250 μm) and shapes (sphere to rectangular) (Figs. 6b, c, 7d and 8b). The carbonate mound facies are sharply overlain by poorly-exposed, organic-rich dolomitic mudstone, which in turn is capped by lithic-rich, compositionally texturally immature sandstone. The highest mounds appear to rise several meters above the level established by the mudstone and sandstone, suggesting that the latter filled in bathymetric relief surrounding the mounds.

4.3. Mineralogy and petrology

The bulk XRD and thin section analyses of all the Little Mesa samples indicates that they are predominantly carbonate, with calcite and dolomite as major phases (Table 2). Calcite crystal size varies from microcrystalline calcite (1–4 μm; Fig. 6b) to microsparspar (5–20 μm, Fig. 8c) and spar (30–100 μm) growth crystals filling gaps. Dolomite crystals ranging from 1 to 50 μm occur as dolomicrite matrix and in pellets, peloids, stromatolite, and algae (Figs. 8a-d). Silicified zones are common (Figs. 8a and 9). They are represented by chert (Fig. 6c), chalcedony (Fig. 6d), and megaquartz that fill void spaces within tubes, between tubes and in the stromatolite buildups (Fig. 6c). Quartz cements occur as fine crystals on the margins of void which increase in size in the center of the voids. Chalcedony forms wedge-like structures where it initiates from the periphery of a void and then widens toward the inside of the void. Chalcedony is distributed throughout micrite and dolomicrite matrix and forms discrete zones in stromatolite buildups (Fig. 6c).

The siliciclastic content of the Little Mesa samples is generally low. Quartz represents on average ~ 5%, and feldspar ~8% (orthoclase) and ~ 4% (albite). This is in agreement with thin section observations. Clay minerals are also low in abundance, consisting entirely of illite with an average abundance of 2.4% (Table 2). A single mudstone sample (LM1–19.2) from within the carbonate-bearing succession is dominated by silicate minerals, including potassium feldspar (40%), clays (16%), and quartz (13%; Table 2; Fig. 6a). This composition might reflect reworking of a volcanic tuff, or else reworking of underlying alluvial siliciclastic facies. Shortite is identified in one sample, $1d_{V1,2}$. Siderite is detected in 3 samples, and a small quantity of hematite was measured in 6 samples at Little Mesa.

4.4. Isotope geochemistry

$\delta^{18}O$ from Little Mesa carbonates ranges from −7.20 to −3.10‰ (and $\delta^{13}C$ ranges from −1.77 to 3.37‰ (VPDB; Table 2). There is no apparent correlation between either oxygen or carbon isotope values and percent carbonate (calcite plus dolomite) measured by XRD ($r = +0.15$, $p = 0.46$, $n = 27$). However, there is a negative correlation between both $\delta^{18}O$ and $\delta^{13}C$ and dolomite ratio dolomite/(dolomite plus calcite) ($r = -0.70$, $p < 0.01$, n = 27 and $r = -0.78$, $p < 0.01$, $n = 27$ respectively; Figs. 10a, b). There also is a strong positive correlation between $\delta^{18}O$ and $\delta^{13}C$ ($r = +0.92$, $p < 0.01$, $n = 27$) (Fig. 10f).

Strontium and rubidium concentrations show a wide variation, with average Sr concentration of 2497 ppm ± 883 S.D. and average Rb concentration of 0.56 ppm ± 0.70 S.D. (Table 2). There is no correlation between Sr concentration and % carbonate ($r = +14$, $p = 0.47$, $n = 27$) or between Rb concentration and % carbonate ($r = -0.13$, $p = 0.51$, $n = 27$). There is also no correlation between Sr concentration and $^{87}Sr/^{86}Sr$ ratio ($r = -0.03$, $p = 0.89$, $n = 27$). $^{87}Rb/^{86}Sr$ ratios vary widely from 0.0001 to 0.0040 with an average of
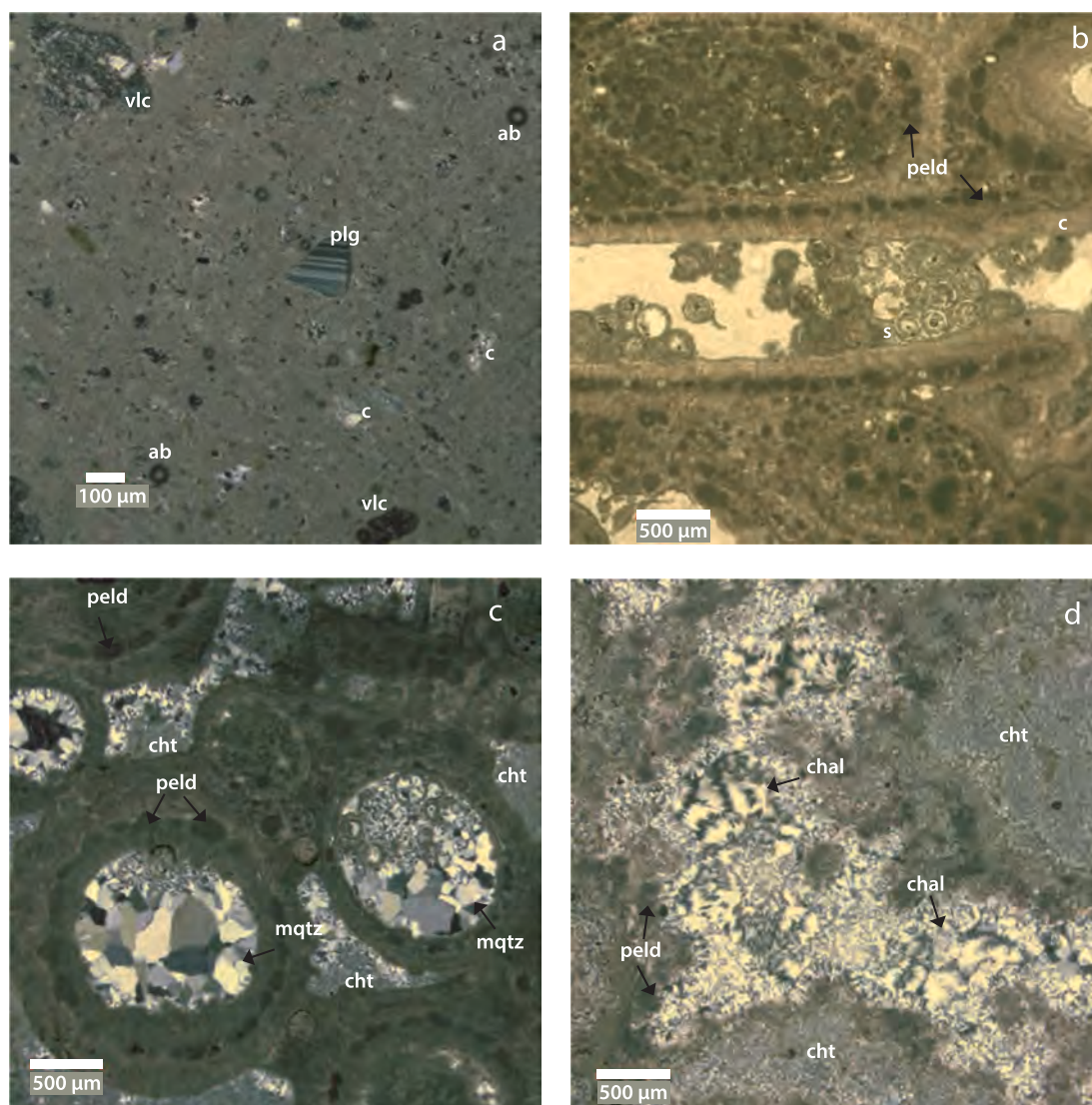
Fig. 6. Cross-polarized light photos of thin sections stained with Alizarin red showing, a) dolomicrite matrix with plagioclase (plg), volcanic clasts (vlc), calcite cement (c), air bubbles (ab), in matrix supported texture, b) calcareous caddis fly larval cases with peloids forming the wall and filling the interior. The caddis fly larval cases also contain spherical structures of uncertain origin (s), peloids (peld), and stained pink calcite cement (c), c) calcareous tube structures with caddis fly larval case walls constructed with peloids (peld); megaquartz (mqtz) and chert (cht) cements filling inside of tubes and void space between tubes, d) silicified micrite to dolomicrite matrix, peloids (peld), and large chert (cht) and chalcedony black arrows (chl) growth to fill voids. (For interpretation of the references to colour in this figure legend, the reader is referred to the web version of this article.)

(0.00068 ± 0.00088 SD; Table 2). These ratios are low, which indicates minimal contamination from silicate minerals in Little Mesa samples. There is no statistically significant correlation between $^{87}Rb/^{86}Sr$ and bulk % XRD carbonate ($r = -0.27$, $p = 0.18$, n = 27). However, there is low negative correlation with % calcite ($r = -0.48$, $p = 0.01$, n = 27) and low positive correlation with dolomite ($r = 0.35$, $p = 0.07$, n = 27).

$^{87}Sr/^{86}Sr$ ratios range from 0.71022 to 0.71140 (Table 2). These ratios are lower than nearly all previously reported data from the Green River Formation in Wyoming (0.71195 to 0.71561) (Table 3; Fig. 11; Doebbert et al., 2014). $^{87}Sr/^{86}Sr$ shows a negative correlation with the dolomite ratio ($r = -0.64$, $p < 0.01$, n = 27) (Fig. 10c). Carbon and oxygen isotopes have a strong positive correlation with $^{87}Sr/^{86}Sr$ ratios (Figs. 10d, e; r = +0.91, p < 0.01, n = 27 and r = +0.86, p < 0.01, n = 27, respectively).

$^{87}Sr/^{86}Sr$ within Sample Set 1 displays a systematic variation with stratigraphic position at Little Mesa. The lowest ratio in this sample group, 0.71022, was measured near the base of the carbonate succession (Fig. 12). Ratios then increase going upward into the upper mounded interval, reaching a maximum of 0.71099 within Sample Set 1, before decreasing again to 0.71060 in the organic-rich mudstone lying above the mounded interval.

Sample Set 2 reveals a wide range of $^{87}Sr/^{86}Sr$ ratios between different mounds in the upper mounded interval, ranging from 0.71064 to 0.71140, with strong positive correlation with $\delta^{18}O$ (Fig. 13). $^{87}Sr/^{86}Sr$ ratios vary across a narrower range of values within individual mounds. Mound 1a, for example, exhibits internal variations between 0.71126 and 0.71140 (Table 2), that correlate with different mound layers (Fig. 9). Tube facies at the center of this mound have the lowest $^{87}Sr/^{86}Sr$ ratios and stromatolite buildups onto tube facies are more radiogenic (Fig. 9).

5. Discussion

5.1. Sedimentary facies evolution

The succession of carbonate facies at Little Mesa is interpreted to record an overall transgression of Lake Gosiute, that may have been

Table 2
Petrographic, mineralogic, and isotopic data.

Sample ID	Component analyzed	Tubes	Stromatolite	spheres	Peoloids	Intraclasts	ostracods	Calcite cement	Silicification	Chalcedony	Megaquartz	% Calcite	% Dolomite	% Quartz	% K-spar	% Albite	% Illite	% Other	$\delta^{18}O$ ‰ (VPD-B)	$\delta^{13}C$ ‰ (VPD-B)	Sr (ppm)	Rb (ppm)	$^{87}Rb/^{86}Sr$	$^{87}Sr/^{86}Sr$
Sample set 1: measured sections																								
LM1–28.8	mudstone											6.6	71.8	2.7	11.1	5.5	2.2	0.0	−7.2	−0.4	6378	1.736-9	0.0008	0.71-060
LM1–25.6$_{Tubes}$	tubes											42.6	46.7	1.2	5.4	2.0	2.0	0.0	−6.4	0.8	2262	0.398-6	0.0005	0.71-099
LM1–25.6$_{Mounds}$	stromatolite											63.7	26.1	1.0	4.0	3.1	2.1	0.0	−4.7	1.8	2663	0.222-9	0.0002	0.71-106
LM1–25.2	grainstone											15.1	55.8	1.7	13.4	12.2	1.7	0.0	−5.1	1.4	2069	2.828-5	0.0040	0.71-096
LM2–23.**6**	stromatolite	No petrographic data										0.8	85.6	1.2	6.6	4.1	1.6	0.0	−6.5	0.2	2448	2.043-1	0.0024	0.71-078
LM2–21.4	stromatolite											30.0	53.3	4.2	6.7	1.7	4.2	0.0	−4.2	2.2	2317	0.932-6	0.0012	0.71-098
LM2–18.6	stromatolite											53.7	25.2	7.6	9.0	1.8	2.7	0.0	−6.8	0.7	1903	0.458-9	0.0007	0.71-070
LM1–19.2	volcanic tuff											11.8	19.8	12.5	39.7	7.4	8.8	0.0	−6.0	0.5	2590	0.925-7	0.0010	0.71-056
LM1–14.10-2	mudstone											22.3	31.4	7.4	29.7	2.5	6.7	0.0	−5.5	−0.9	710	0.333-7	0.0014	0.71-022
Sample set 2: mounds																								
1a$_{II1}$	stromatolite		●		●			●	●			40.8	33.7	16.5	4.8	4.1	0.0	0.0	−3.7	2.9	2060	0.118-1	0.0002	0.71-133
1a$_{II2}$	stromatolite		●		●			●	●	●		35.4	34.8	17.8	6.8	5.2	0.0	0.0	−3.5	3.1	1992	0.106-1	0.0002	0.71-132
1a$_{II3}$	stromatolite	●	●		●			●	●			53.8	29.3	4.7	6.9	4.3	0.0	1.0	−3.3	3.2	2576	0.152-3	0.0002	0.71-133
1a$_{III1}$	tubes	●						●	●	●		64.7	22.9	1.4	4.6	6.4	0.0	0.0	−3.5	3.1	2606	0.251-7	0.0003	0.71-139
1a$_{III2}$	stromatolite		●		●			●	●	●		58.6	29.5	1.6	4.0	2.1	0.0	4.3	−3.1	3.4	2476	0.311-9	0.0004	0.71-139
1a$_{III3}$	stromatolite		●					●	●	●	●	55.1	34.0	1.4	2.6	3.8	3.0	0.0	−3.3	3.0	2523	0.249-2	0.0003	0.71-135
1a$_{IV}$	stromatolite	●	●	●	●			●	●	●	●	52.6	33.9	1.2	2.6	3.9	3.1	2.7	−3.2	3.2	2616	0.179-9	0.0002	0.71-138
1a$_{Tubes}$	tubes	●	●					●				23.8	66.2	3.3	5.0	1.1	0.6	0.0	−3.8	2.1	2275	0.532-2	0.0007	0.71-126
1a$_{V}$	stromatolite		●		●			●	●	●	●	67.7	22.0	0.9	2.4	4.4	2.6	0.0	−3.3	3.1	2636	0.173-5	0.0002	0.71-140
1b$_{1,2}$	stromatolite		●	●	●		●	●	●	●	●	4.0	80.4	3.5	6.0	2.7	1.8	1.6	−6.5	0.3	2526	0.593-0	0.0007	0.71-077
1c	stromatolite			●	●	●	●	●	●	●		4.5	83.5	0.6	5.5	3.0	2.0	1.0	−5.5	0.1	2468	0.178-4	0.0002	0.71-073
1d$_{VI1,2}$	stromatolite		●		●		●	●	●	●	●	1.1	79.2	0.3	8.1	4.4	2.2	4.7	−7.1	−1.8	2854	0.161-4	0.0002	0.71-064
1d$_{VII}$	stromatolite		●	●	●		●	●				1.3	88.0	1.0	6.6	1.9	1.3	0.0	−6.5	−1.4	2445	1.650-3	0.0020	0.71-071
1e$_{III1,2}$	stromatolite	●	●	●			●	●		●		6.1	84.5	1.7	3.9	1.5	2.3	0.0	−5.1	1.0	1779	0.048-4	0.0001	0.71-086
1f	stromatolite	●	●					●	●	●	●	58.0	35.6	0.6	2.5	1.3	2.0	0.0	−4.5	1.9	2549	0.156-8	0.0002	0.71-108

8

Table 2 (continued)

Sample ID	Component analyzed	Tubes	Stromatolite	spheres	Peloids	Intraclasts	ostracods	Calcite cement	Silicification	Chalcedony	Mega-quartz	% Calcite	% Dolomite	% Quartz	% K-spar	% Albite	% Illite	% Other	δ18O ‰ (VPDB)	δ13C ‰ (VPDB)	Sr (ppm)	Rb (ppm)	87Rb/86Sr	87Sr/86Sr
2a$_{1,2}$	wackestone	●	●		●	●	●	●				60.7	27.5	3.5	5.3	1.5	1.5	0.0	−4.2	2.6	2835	0.256-9	0.0003	0.71-103
2b1$_{1,2}$	stromatolite	●	●					●	●	●		53.9	16.6	15.0	5.8	4.1	4.6	0.0	−3.6	3.2	2329	0.042-5	0.0001	0.71-132
2b$_2$	stromatolite		●		●			●	●			56.5	12.3	13.6	9.7	1.3	6.5	0.0	−3.6	3.2	2526	0.063-1	0.0001	0.71-129

Notes: 1σ error in δ18O and δ13C < 0.1 ‰.
2σ error in 87Sr/86Sr ratios for all samples is ± 0.00001.

punctuated by several smaller, higher-frequency transgressions and regressions (Leggitt and Cushman Jr, 2001; Seard et al., 2013; Fig. 3). Shingled low-relief bedforms near the base of this succession are interpreted to record lateral to downstream accretion of carbonate intraclasts, transported by unidirectional currents moving through a palustrine plain (c.f. Arenas et al., 2007; Arenas-Abad et al., 2010). Trough cross-bedded grainstone intervals higher in the succession could reflect either fluvial or shoreface reworking. The largest mounds, found near the top of the carbonate succession, are interpreted to represent the deeper littoral to sub-littoral environments, based on the relief on the largest mounds (and assuming they were entirely subaqueous). Evidence for breakage and toppling of these mounds suggests that they were impacted by relatively high-energy waves, or alternatively were damaged during earthquakes (cf. Törő and Pratt, 2015).

Previous studies have interpreted the organic-rich dolomitic mudstone capping the Little Mesa mounds as the basal Laney Member (Roehler, 1989; Leggitt and Cushman Jr, 2001; Seard et al., 2013). We interpret is as part of the Wilkins Peak Member however, for two reasons. First, it lacks fish fossils, which are common in the Laney Member. Second, its ^{87}Sr/^{86}Sr ratio (0.71060) is much lower than the basal Laney Member near the basin center (> 0.71400, see Fig. 14). The lithic-rich sandstone capping the succession is interpreted as volcaniclastic detritus of the Sand Butte Bed of the Laney Member, in agreement with previous studies (e.g., Roehler, 1989).

5.2. Little Mesa isotopic evolution

Several lines of evidence suggest that isotopic values in Little Mesa carbonate minerals retain an isotopic record influenced either by primary precipitation, or else by penecontemporaneous diagenesis. First, the juxtaposition of calcite and dolomite lamina at the sub-mm scale in some stromatolite samples precludes wholesale recrystallization of carbonate within these relatively dense facies. Second, different ^{87}Sr/^{86}Sr values are preserved in different mound layers (Fig. 9), suggesting that they too have not been pervasively altered. Third, δ^{13}C, δ^{18}O, and ^{87}Sr/^{86}Sr vary widely between different mounds sampled above the tuff marker bed. Fourth, Little Mesa carbonate facies exhibit strong linear covariance of δ^{13}C and δ^{18}O (Fig. 10). This relationship is difficult to explain as the result of interaction between carbonate minerals, which contain C and O at a 1:3 M ratio, and diagenetic water in which the C:O ratio is much smaller. Banner and Hanson (1990) calculated that δ^{18}O in carbonate minerals equilibrates with diagenetic fluids at water/rock ratios three orders of magnitude less than required for δ^{13}C. If primary carbonate minerals at Little Mesa were enriched in ^{13}C and ^{18}O, progressive diagenetic alteration should initially be marked by a large negative shift in δ^{18}O, accompanied by a smaller change in δ^{13}C. Only after δ^{18}O has approached equilibrium should exchange with diagenetic fluids be able to drive δ^{13}C to lower values. The expected trend associated with meteoric diagenesis therefore is not a linear mixing line, but rather an "inverted J" (e.g., Lohmann, 1988; Bishop et al., 2014).

Covariant trends with slopes similar to that at Little Mesa have previously been observed in many other lacustrine carbonate deposits, and have been interpreted as primary signals related to evaporation within hydrologically closed lake basins (Talbot, 1990; Li and Ku, 1997; Horton et al., 2016). Increased evaporation can cause δ^{18}O to be more positive due to preferential loss of ^{16}O to the vapor phase, while degassing of CO_2 or photosynthesis from the lake surface results in preferential loss of ^{12}C, resulting in higher δ^{13}C in the lake. δ^{13}C may be further influenced by changes in lake productivity, which may correlate with salinity in a closed basin (e.g., McKenzie, 1985; Jellison et al., 1996).

Because Sr isotopes are not fractionated by meteoric or biologic processes, the observed variation in ^{87}Sr/^{86}Sr cannot be explained by mechanisms involving changing evaporation or productivity. Instead, we propose that this covariance reflects varying degrees of mixing
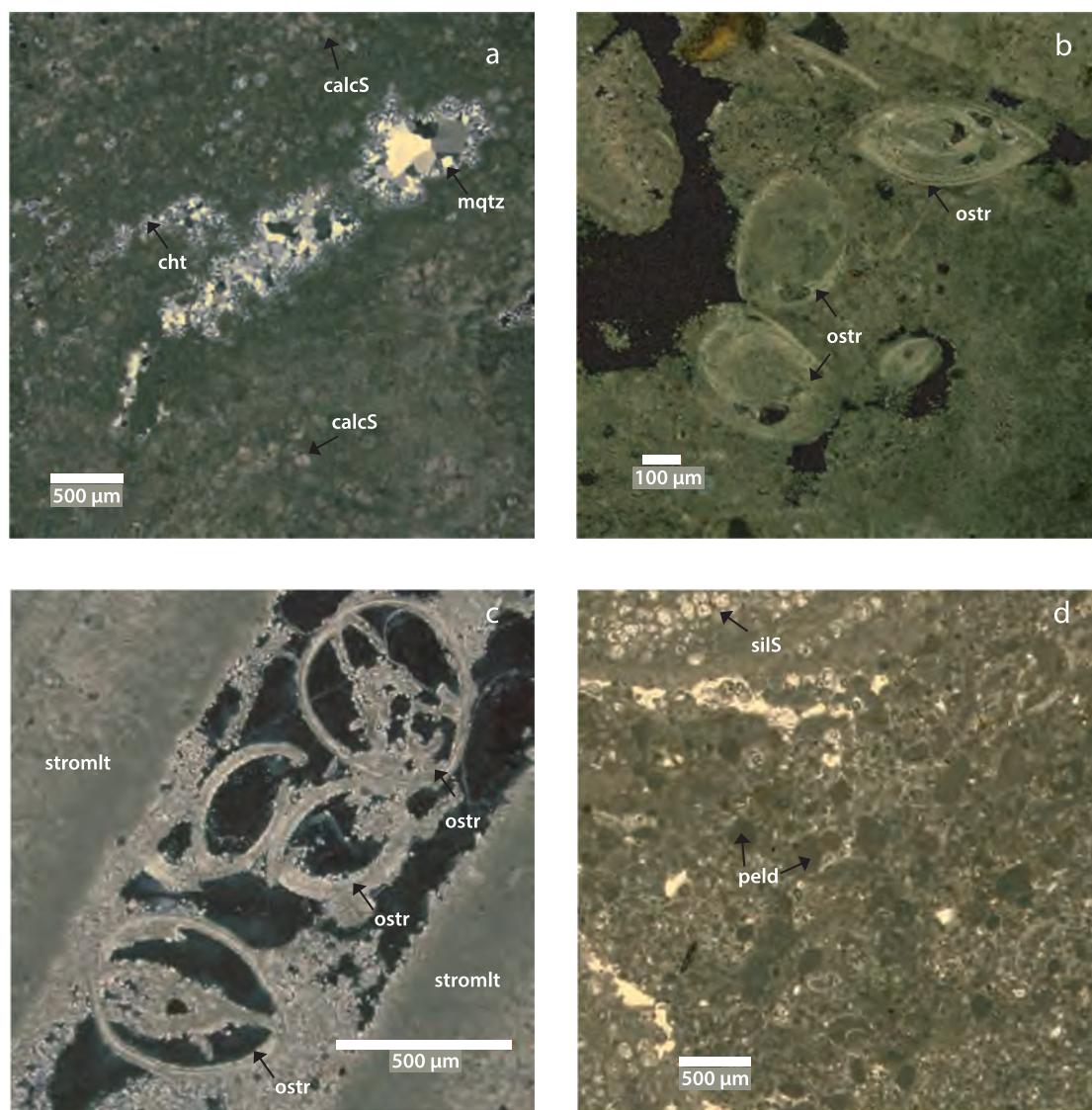
Fig. 7. Cross-polarized light photos of thin sections stained with Alizarin red showing, a) megaquartz (mqtz) and chert (cht) crystal filling the voids within stromatolite as well as calcareous spheres (calcS), b) lacustrine arthropods probably ostracods (ostr) with thick wall scattered in dolomicrite matrix with dolomitic shells, c) large lacustrine ostracods (ostr) scattered in voids between digitate stromatolite (stromlt), d) peloids of different sizes and shapes filling between stromatolite digitate and siliceous spheres (silS). (For interpretation of the references to colour in this figure legend, the reader is referred to the web version of this article.)

between lake water and groundwater. This groundwater is inferred to have had relatively low $^{87}Sr/^{86}Sr$, due to the influence of marine carbonate lithologies that are common in the adjacent fold and thrust belt to the west (Rhodes et al., 2002; Bataille and Bowen, 2012; Doebbert et al., 2014; Baddouh et al., 2016). The observed $\delta^{18}O$ minimum near −7‰ is broadly consistent with even more negative meteoric waters, that experienced evaporation in the lake (Doebbert et al., 2010). $\delta^{13}C$ in groundwater was likely also below 0 if it contained significant organic-respired CO_2. In contrast, Lake Gosiute water on the whole had higher $^{87}Sr/^{86}Sr$ due to drainage from bounding Laramide uplifts (Rhodes et al., 2002; Doebbert et al., 2014). Lake water $\delta^{13}C$ and $\delta^{18}O$ values were likely enriched due to greater evaporation and organic matter burial, as noted in previous studies (e.g. McKenzie, 1985; Talbot, 1990; Horton et al., 2016).

Surprisingly, dolomite ratio (dolomite/(dolomite plus calcite)) exhibits a negative correlation with all three reported isotopic values (Fig. 10). The origin of the dolomite is uncertain. Dolomite is common in Green River Formation lacustrine mudstone and is a major constituent of the Wilkins Peak Member (Mason, 2012; Baddouh et al., 2017). Several different mechanisms for its origin have been proposed.

Wolfbauer and Surdam (1974) argued that dolomitization in the Laney Member in the Bridger Basin occurred beneath lake-fringing mudflats, due to evaporative concentration of Mg-rich subsurface brines. Desborough (1978) proposed that Mg was concentrated in cyanobacteria in the water column and buried in lake-floor mudstone in the Piceance basin, where its release during organic matter decay resulted in dolomitization of calcite. Eugster and Hardie (1975) and Smoot (1983) proposed a syndepositional clastic origin for Wilkins Peak Member dolomite, in which intraclasts derived from fringing mudflats were transported toward the basin depocenter.

None of the above models appear satisfactory to explain mm-scale juxtaposition of calcite and dolomite within lake-margin tufa and stromatolite facies, and models involving evaporative concentration conflict with the observed negative correlation between dolomite and $\delta^{18}O$ at Little Mesa. Gebelein and Hoffman (1973) proposed that mm-scale dolomite lamina in stromatolite may form diagenetically during the decomposition of Mg-enriched cyanobacterial lamina. However, penecontemporaneous dolomite has also been reported from late Cenozoic tufa deposits in the western U.S. (Benson, 1994; Pedone and Dickson, 2000). Pedone and Dickson (2000) posited that poorly ordered
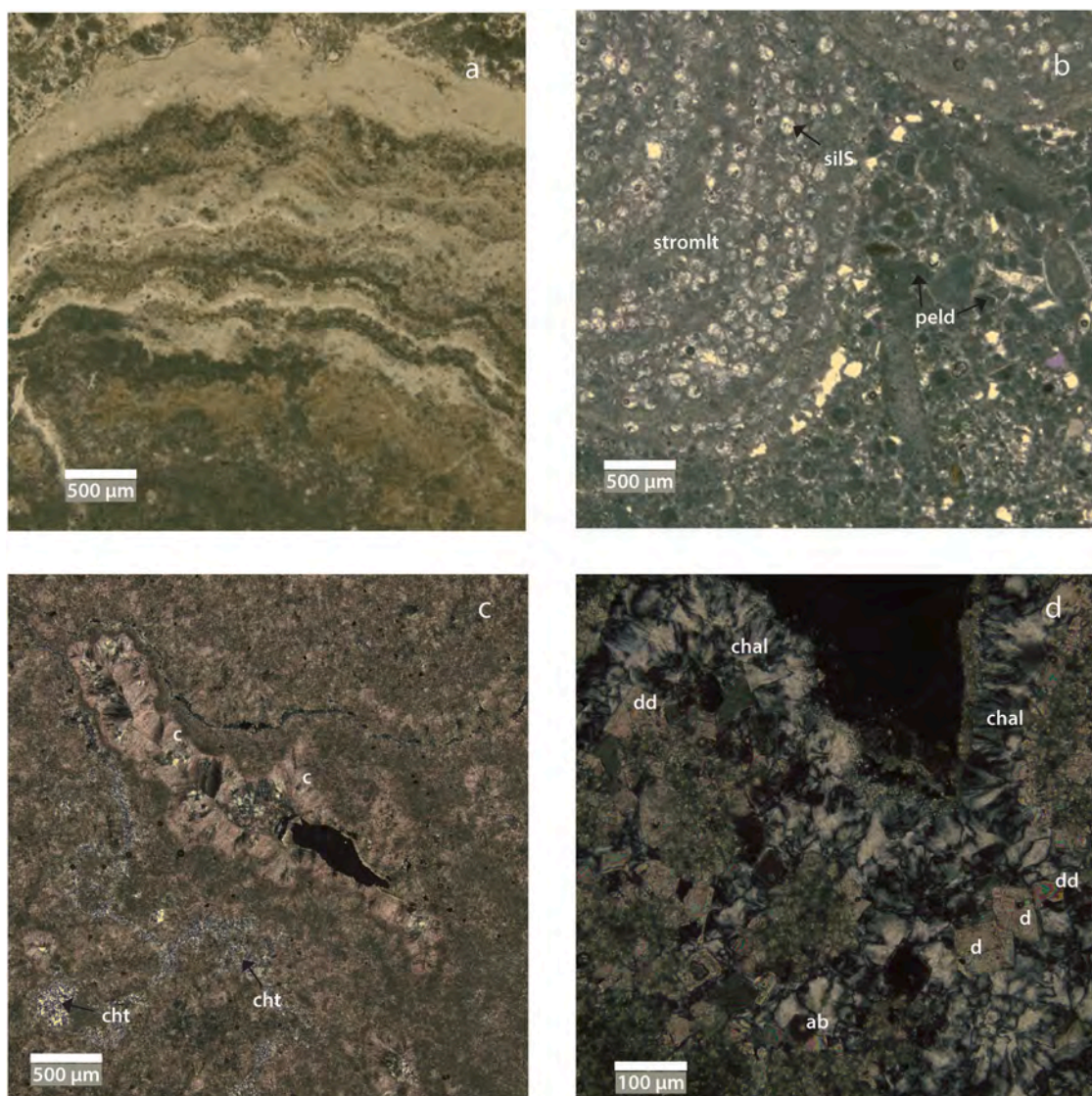
Fig. 8. Cross-polarized light photos of thin sections stained with Alizarin red showing, a) silicified planar laminated stromatolite, b) digitate stromatolite with siliceous spheres (silS) and peloids (peld) filling between digitate structures, c) stained red microcrystalline calcite to spar; note calcite crystal growth filling the gaps, note chert (cht) zone in lower left, d) Not stained dolomite crystals that makes dolomicrite matrix, notice silicified zones with large chalcedony growth (chal) to fill voids as well as single euhedral dolomite (d) and de-dolomite (dd). (For interpretation of the references to colour in this figure legend, the reader is referred to the web version of this article.)

dolomite in Great Salt Lake tufa resulted from dissolution of primary aragonite by a fluid that incorporated Mg from lake water and was supersaturated with respect to dolomite.

The data reported here suggest that groundwater influx contributed to dolomite oversaturation at Little Mesa, either directly or when mixed with lake water.

Recent studies suggest that primary dolomite precipitation may also be mediated by biofilms (e.g., García del Cura et al., 2014; Gelband et al., 2019). García del Cura et al. (2014) inferred some biogenic influence on δ^{13}C in calcite, but concluded that.

δ^{18}O is determined primarily by climatic conditions. Gelband et al. (2019) noted that δ^{18}O values in Miocene microbially-mediated dolostone in northern Israel are significantly higher than those in limestone, and they concluded that the higher values reflected elevated salinity and enhanced evaporation. This observation stands in contrast to the lower δ^{18}O values in Little Mesa dolomite compared to calcite.

Based on detailed examination of one representative mound (Fig. 9), tube structures, which represent the core of most the large and small mounds are less radiogenic than stromatolite immediately covering them.

The concentric structure of the mounds consistently indicates the formation of the tube structures predated the initiation of stromatolite formation, which implies that isotopic composition of carbonate-precipitating waters changed through time. The most likely scenario is that the tubes were more strongly influenced by groundwater discharge, whereas the more radiogenic stromatolite facies were more strongly influenced by lake water. Alternatively, this change could reflect an increase in more radiogenic surface drainage into the lake (c.f., Rhodes et al., 2002; Doebbert et al., 2014). It is also possible that the more porous tube facies was disproportionately influenced by later diagenesis, or that the single mound examined in detail is not representative of others.

5.3. Relationship to basin-center lacustrine deposits

Interpreting the broader paleo-limnologic significance of Little Mesa carbonate facies requires a detailed understanding of the stratigraphic relationship of these basin-marginal deposits to other Lake Gosiute facies deposited closer to the center of the Bridger Basin. We conclude that the Little Mesa facies correlate with the upper part of the Wilkins

Fig. 9. Cross-cut of calcareous mound showing the measured $^{87}Sr/^{86}Sr$ ratios of different layers in the mound. Arrow indicates up direction. Caddis fly larval cases form core of the mound, which is surrounded by successive stromatolite layers.

Peak Member. Two important lines of evidence support this interpretation. First, the Little Mesa "tuff marker bed" observed in this and previous studies (Leggitt and Cushman Jr, 2001; Seard et al., 2013) appears physically similar to the "5th Tuff" of Culbertson (1961), which later became known as the "Layered Tuff" due to its distinctive internal stratigraphy (Roehler, 1989, 1992). At the city of Green River in Wyoming, the Layered Tuff occurs ~30 m below the top of the Wilkins Peak Member (Culbertson, 1961; Smoot, 1983; Roehler, 1992; Pietras and Carroll, 2006). It has been dated at 50.12 ± 0.09 Ma based on $^{40}Ar/^{39}Ar$ in sanidine (Smith et al., 2003, 2008, 2010) and 49.919 ± 0.040 using U−Pb in zircon (Machlus et al., 2015). The greater thickness of the Little Mesa marker tuff compared to the Layered Tuff at Green River (~115 km south) is consistent with the closer proximity of Little Mesa to active volcanic centers to the north and northwest of the Bridger Basin (c.f., Smith et al., 2008). If the Little Mesa and Layered Tuffs do represent the same eruptive event, then the

Little Mesa carbonate facies must be equivalent to the upper Wilkins Peak member, and not the lower Laney Member as earlier interpreted (Roehler, 1993; Leggitt and Cushman Jr, 2001; Seard et al., 2013).

The second line of evidence supporting correlation of the Little Mesa carbonate facies to the Wilkins Peak Member comes from Sr isotope ratios. $^{87}Sr/^{86}Sr$ in Little Mesa carbonate facies is lower than in nearly all other samples from the Green River Formation (Doebbert et al., 2014; Fig. 9). The lowest $^{87}Sr/^{86}Sr$ in basin-center deposits occurs within the Wilkins Peak Member however, within a few meters of the level of the Layered Tuff (Fig. 14). Pietras (2003) and Baddouh et al. (2016, 2017) noted that $^{87}Sr/^{86}Sr$ in Wilkins Peak Member lake cycles is strongly correlated with facies evidence for water depth, with the lowest ratios found in organic-rich mudstone deposited during lake highstands. Relatively low $^{87}Sr/^{86}Sr$ at Little Mesa is therefore consistent with the prediction that the carbonate deposits record expansion and transgression of Lake Gosiute.
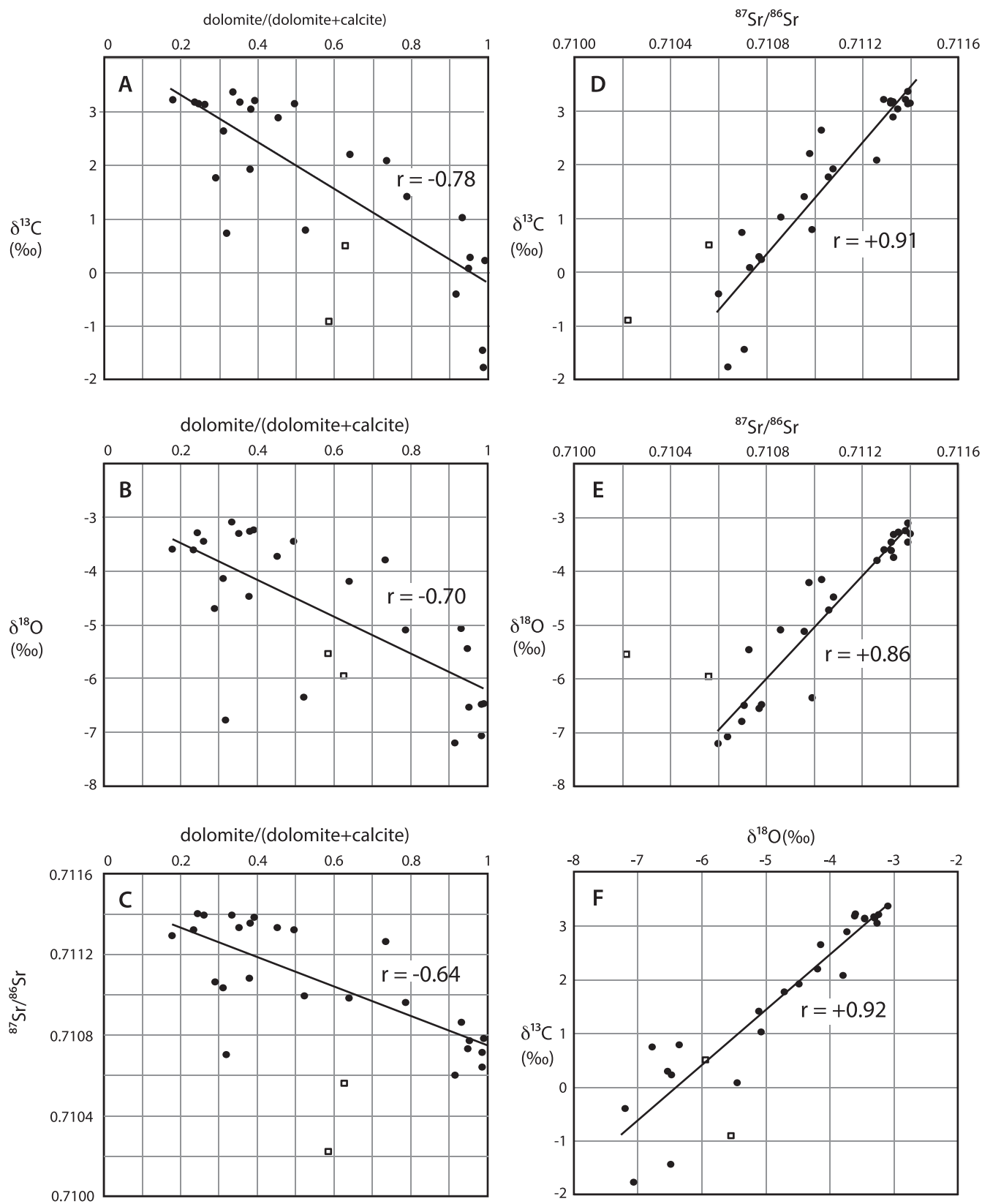
Fig. 10. Cross-plots of Little Mesa dolomite ratio, $\delta^{13}C$, $\delta^{18}O$, and $^{87}Sr/^{86}Sr$ for all samples. Open squares indicate samples near base of carbonate interval that contain > 46% silicate minerals.

Table 3
Measured Rb–Sr isotope data and percent carbonate for the carbonate fraction from mudstone in the White Mountain #1 drill core.

	White Mountain-1 Core ($n = 48$)		Little Mesa Outcrops (n = 27)	
	Average	*Std. Dev.*	Average	*Std. Dev.*
% Carbonate	48.6	*18.5*	80.6	*13.4*
% Calcite	24.5	*23.2*	35.0	*24.1*
% Dolomite	25.0	*13.6*	45.5	*24.9*
% Shortite	0.5	*1.7*	0.1	*0.5*
% Quartz	10.9	*4.8*	4.7	*5.4*
% Othoclase	18.6	*11.1*	8.1	*8.2*
% Albite	4.2	*2.1*	3.6	*2.4*
% Illite	14.9	*12.5*	2.4	*2.2*
% Montmorillonite	0.9	*2.1*	0.0	*0.0*
% Siderite	0.1	*1.0*	0.2	*0.6*
% Hematite	0.4	*0.6*	0.3	*0.5*
Rb (ppm)	0.60	*0.37*	0.56	*0.70*
Sr (ppm)	1532	*481*	2497	*883*
$^{87}Rb/^{86}Sr$	0.00117	*0.00085*	0.00070	*0.00088*
$^{87}Sr/^{86}Sr$	0.71267	*0.00062*	0.71102	*0.00033*
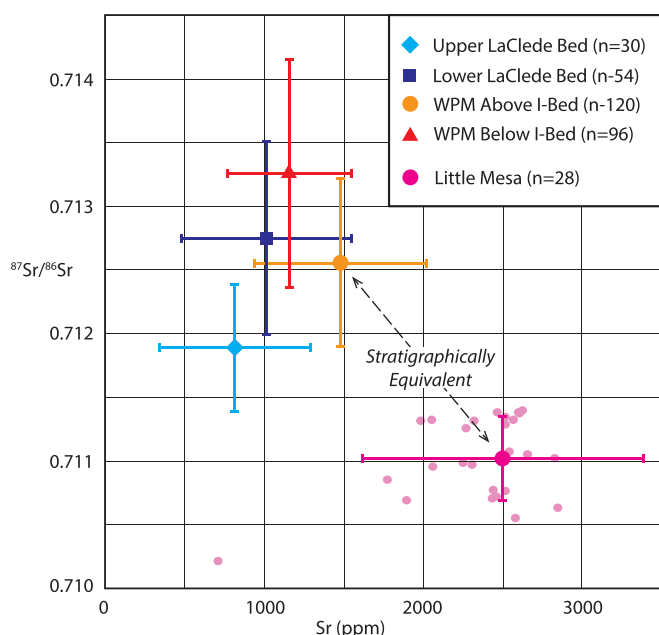
Fig. 11. Summary of Wilkins Peak and Laney Member Sr concentration and $^{87}Sr/^{86}Sr$ measure on primary carbonate in lacustrine mudstone (data reported by Rhodes et al., 2002; Doebbert et al., 2014; Baddouh et al., 2016, 2017, and this study). Little Mesa samples are stratigraphically equivalent to the upper Wilkins Peak Member above sandstone marker bed I. Error bars indicate ± 1 SD about the mean for each stratigraphic unit.

Our results conflict with previous studies that correlated the Little Mesa deposits to the Laney Member (Roehler, 1989; Leggitt and Cushman Jr, 2001; Leggitt and Loewen, 2002; Seard et al., 2013). The Laney Member does record an abrupt, fundamental transition to a more persistently deep lake, as evidenced by the deposition of fish-bearing organic-rich mudstone (e.g., Rhodes and Carroll, 2015; Carroll, 2017). Numerous intervals of similarly organic-rich mudstone also occur within the Wilkins Peak Member however (e.g., Roehler, 1992; Pietras and Carroll, 2006; Johnson et al., 2011). This conclusion is reinforced by $^{87}Sr/^{86}Sr$ near the basin-center, which increases sharply at the transition from the Wilkins Peak Member to the Laney Member, in contrast to relatively low $^{87}Sr/^{86}Sr$ of Little Mesa carbonate and organic-rich mudstone (Figs. 12, 14).

The detailed correlation of the Little Mesa carbonate interval to

high-frequency lake expansion-contraction cycles observed near the basin center is less clear. The entire Little Mesa interval may correspond to a single precessional cycle (Fig. 12, interpretation "A"; Baddouh et al., 2016), which would imply that the carbonate mound interval is expanded in thickness by approximately 10× compared to its downdip equivalent. While this would require relatively high net accumulation rates at Little Mesa (averaging several mm/yr), Quaternary mound complexes of similar or greater thickness were deposited in Pyramid and Searles lakes over time scales of ~20 kyr or less (e.g., Benson, 2004; Smith, 2009). Alternatively, the Little Mesa interval could represent a ~ 100 kyr eccentricity cycle that encompasses 5 precessional-scale lake expansion-contraction cycles downdip (Fig. 12, interpretation "B"; Aswasereelert et al., 2013). In this case the time-equivalent up-dip and downdip intervals could be similar in thickness.

5.4. Hydrologic evolution of Eocene Lake Gosiute

Although Little Mesa carbonate strata correlate with the least radiogenic facies of the upper Wilkins Peak Member, the highest measured $^{87}Sr/^{86}Sr$ ratios at Little Mesa are lower than nearly all $^{87}Sr/^{86}Sr$ measurements made on lacustrine mudstone near the basin center (Fig. 11). We therefore infer that the Lake Gosiute Sr isotopic reservoir was not fully mixed, and that active influx of groundwater and surface runoff from the north maintained either a localized lateral geochemical gradient within the lake, stratification into more radiogenic and less radiogenic layers, or both. Geochemical gradients are known to occur where rivers enter very shallow hypersaline lakes (e.g., Emdadi et al., 2016), and can also result from spring discharge. For example, Nasikie Engida in southern Kenya receives most of its water from perennial northern hot springs. During the summer of 2006 its salinity increased eight-fold from its northern to its southern shores, a distance of ~6 km (Renaut et al., 2020). Stratification (meromixis) commonly occurs in deeper lakes due to hypopycnal flow of fresh surface water over more saline bottom waters (cf. Awramik and Buchheim, 2015). Based on presently available data we are not able to quantify the relative importance of groundwater versus surface runoff in maintaining a geochemical gradient in Lake Gosiute, but the widespread distribution of the carbonate facies similar to Little Mesa suggests that the groundwater contribution was significant.

The highest $^{87}Sr/^{86}Sr$ ratios at Little Mesa occur within the upper mounded facies. This observation initially appears to directly conflict with the observation that the lowest $^{87}Sr/^{86}Sr$ ratios in the central and southern Bridger Basin occurred during highstands, which are marked by oil shale beds (Fig. 12; Rhodes et al., 2002; Pietras, 2003; Baddouh et al., 2016, 2017). The dilemma may be resolved however by considering how Lake Gosiute may have evolved as lake level changed.

Fig. 15 presents a schematic model for $^{87}Sr/^{86}Sr$ compositions that is based on mixing of two distinctly different water sources during transgression. The first is runoff and spring discharge of waters derived from the Cordilleran orogen to the west. These waters are inferred to have had relatively low $^{87}Sr/^{86}Sr$ due to interaction with marine limestone within the Sevier fold and thrust belt (Gierlowski-Kordesch et al., 2008; Bataille and Bowen, 2012; Doebbert et al., 2014). The second source is Laramide foreland uplifts that lie to the north, east, and south of the basin. These waters are inferred to have been more radiogenic due to weathering of Precambrian basement rocks and to the diminished thickness of marine carbonate strata compared to the fold and thrust belt. In addition to uplifts that directly about the Green River basin, recent detrital zircon age analyses have shown that Lake Gosiute also received drainage from more distant sources in central Colorado (Hammond et al., 2019). Modern river water obtained from streams draining the Sevier fold and thrust belt versus Laramide uplifts confirm that they have distinctly different $^{87}Sr/^{86}Sr$ ratios (Doebbert et al., 2014).

The relative importance of these two sources in determining Lake Gosiute $^{87}Sr/^{86}Sr$ is uncertain because the Sr concentrations of influent
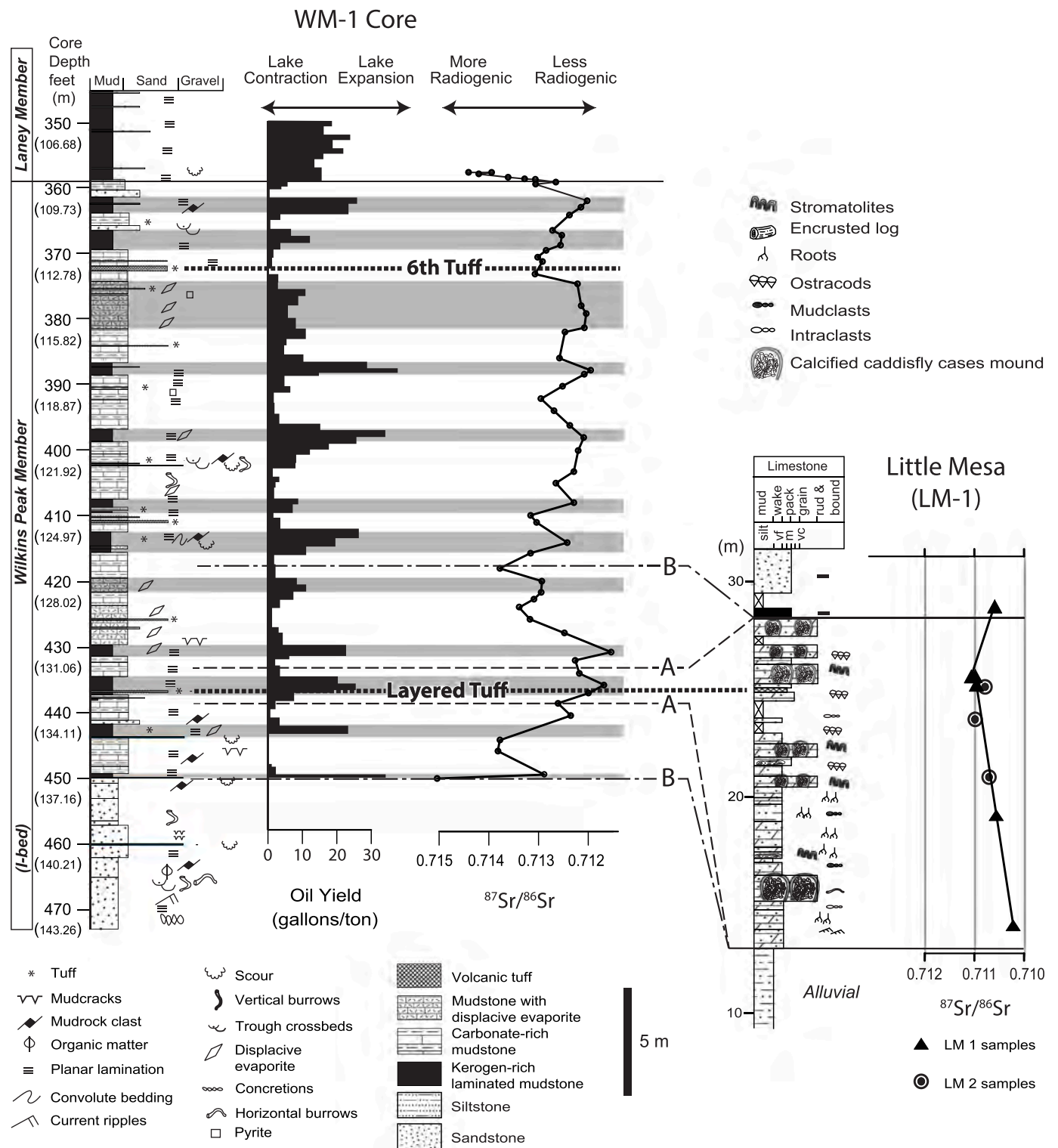
Fig. 12. Correlation between Little Mesa and White Mountain core using the Layered Tuff as a datum. Dashed lines labeled A and B represent alternative correlations of the Little Mesa interval to the core based on oil yield, and layered Tuff as well as Sr isotopes (this study). Gray shading is interpreted to represent lake highstands as previously associated with high oil yield and less radiogenic Sr isotopes (Baddouh et al., 2017). Oil yield based on Fisher assay analyses (U.S. Geological Survey Oil Shale Assessment Team, 2008).

waters are unknown. However, lake level rise appears to have coincided with a disproportionately large increase in Sr derived from the first source than from the second, in response to increased precipitation of Pacific-derived moisture onto the Cordilleran orogen (c.f., Smith et al., 2014; Baddouh et al., 2016, 2017). Prior to deposition of Little Mesa carbonate this influx was relatively small (Fig. 15a). It subsequently

increased, resulting in lake level rise and the deposition of spring deposits with low $^{87}Sr/^{86}Sr$ along the northwestern lake margin (Fig. 15b). Near Little Mesa the lake is inferred to have been very shallow during this stage, on the order of a few meters. A lateral geochemical gradient was re-established between less radiogenic lake waters near Little Mesa and more radiogenic waters near the lake
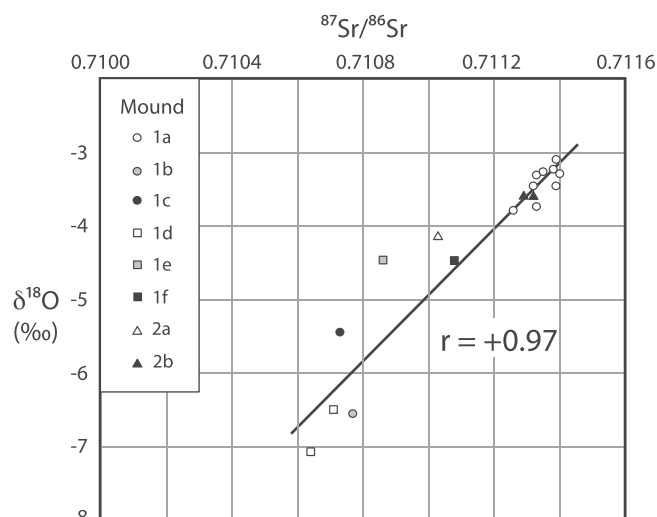
Fig. 13. Cross-plot of $\delta^{18}O$ versus $^{87}Sr/^{86}Sr$ for only individual Little Mesa mounds above tuff marker bed. Notice stronger ($r^2 = 0.93$) positive correlation between strontium and oxygen isotopes compared to cross-plot10E ($r^2 = 0.89$). See Table 2 for detailed mineralogy of these samples.
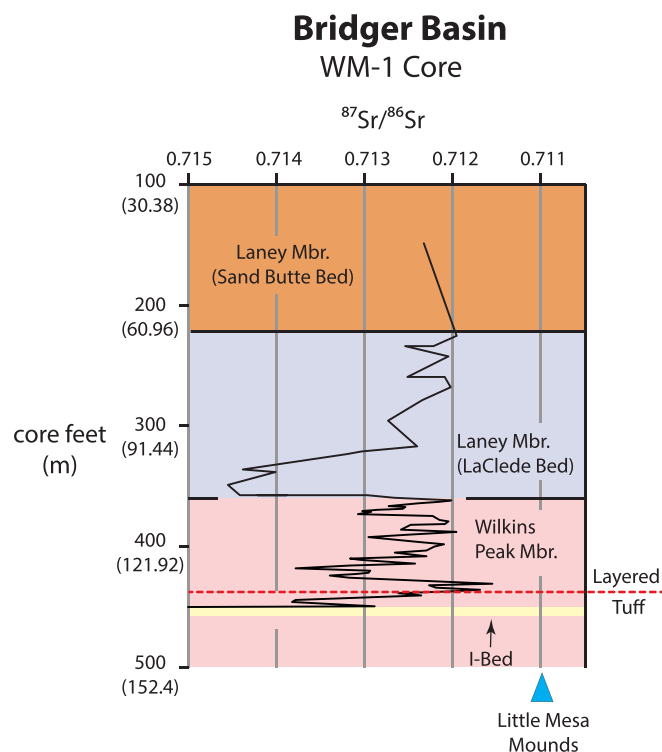

Fig. 14. Trend of Sr isotopes in WM-1 core measured in Upper Wilkins Peak Member and Lower Laney Member (data reported by Doebbert et al., 2014; Baddouh et al., 2016, 2017). Notice the lowest $^{87}Sr/^{86}Sr$ in basin-center deposits occurs within the Wilkins Peak Member, within a few meters of the level of the Layered Tuff in contrast to more radiogenic $^{87}Sr/^{86}Sr$ ratios in the Laney Member.

of hypopycnal flow from the northwest with similar flows coming from other, more radiogenic sources and with more saline waters below the chemocline. Lake surface water at the basin center remained more radiogenic than any waters at Little Mesa however. Fluctuation in the position of the chemocline at Little Mesa may have been responsible for the strong positive covariance of $\delta^{18}O$, $\delta^{13}C$, and $^{87}S/^{86}Sr$ within the upper mound facies.

6. Conclusions

The combination of tuff stratigraphy, $^{87}Sr/^{86}Sr$, $\delta^{13}C$, and $\delta^{18}O$ of mounded lacustrine carbonate at Little Mesa reveals details of the paleolimnology and paleohydrology of Eocene Lake Gosiute that would not be apparent using any of these approaches alone. In contrast to earlier interpretations that these facies were deposited during a relatively deep, balanced-fill lake phase represented by the Laney Member, we conclude that they in fact correspond to the underfilled phase recorded by the Wilkins Peak Member. As such, they may be broadly similar in origin to similar Quaternary carbonate tufa facies reported from the Great Basin region that are known to have been strongly influenced by groundwater discharge during lake highstands. Comparison of $^{87}Sr/^{86}Sr$ in Little Mesa carbonate to downdip deposits near the basin center suggests the presence of a localized lateral geochemical gradient, in a lake that episodically expanded and contracted across a low-gradient basin floor.

Little Mesa mound facies exhibit a strong covariance between $\delta^{13}C$ and $\delta^{18}O$, a feature commonly associated with hydrologically closed lakes. Such covariance is typically attributed to a combination of evaporative fractionation at the lake surface and evaporation-driven changes in paleoproductivity. In Little Mesa samples $\delta^{13}C$ and $\delta^{18}O$ also covary with $^{87}Sr/^{86}Sr$, which has not been previously reported and which cannot be explained solely by meteoric processes. We instead propose that these relationships at Little Mesa reflect variable mixture of lake water with groundwater (spring) influx. Lake water was enriched in ^{87}Sr due to drainage from highly radiogenic Precambrian-cored uplifts, and in ^{13}C and ^{18}O due to evaporation. Groundwater was isotopically depleted due by interaction with marine carbonate lithologies contained within the Sevier fold and thrust belt. Mixing of lake water with groundwater may represent an underappreciated contributor to stable isotopic covariance in other ancient lake carbonates as well (cf. Hudson et al., 2017)

Declaration of Competing Interest

There is no confect of interest associated with this publication and data used.

center. Limited mixing across this gradient resulted in a decrease in lake center $^{87}Sr/^{86}Sr$ from its original ratio. Further increase in Cordilleran precipitation caused additional lake-level rise (Fig. 15c). The lateral geochemical gradient transitioned into hypopycnal flow and the establishment of salinity stratification, in a lake that was on the order of 10 m deep at Little Mesa (cf. Awramik and Buchheim, 2015). Lake center surface water became less radiogenic due to progressive mixing
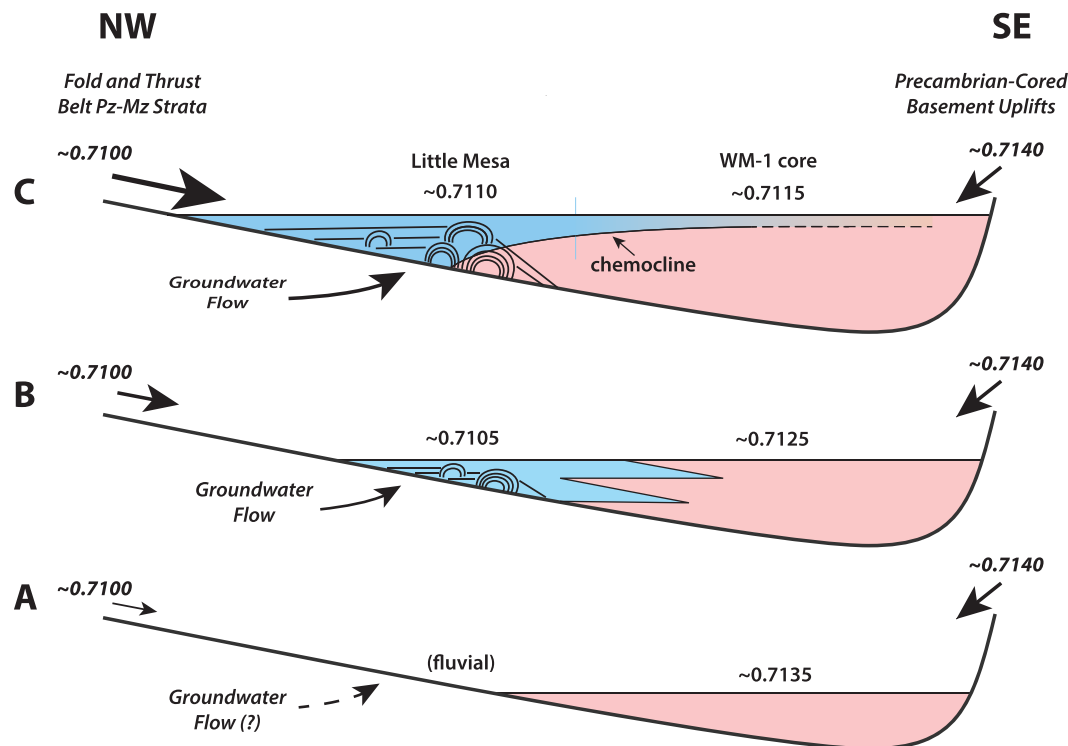
Fig. 15. Schematic model for mixing of different water sources in Lake Gosiute during lake transgression and concurrent changes in $^{87}Sr/^{86}Sr$ in lacustrine carbonate (not to scale). WM-1 = White Mountain #1 core (Figs. 1, 12). Arrows indicate surface runoff and spring discharge to the lake. Sawtooth line denotes a localized lateral geochemical gradient related to influx of fresh water into northwest corner of Bridger Basin. See text for further discussion.

Appendix A. Supplementary data

Supplementary data to this article can be found online at https://doi.org/10.1016/j.palaeo.2020.110038.

References

Desborough, G.A., 1978. A biogenic-chemical stratified lake model for the origin of oil shale of the Green River Formation; an alternative to the playa-lake model. Geol. Soc. Am. Bull. 89, 961–971.

U.S. Geological Survey Oil Shale Assessment Team, 2008. Fischer Assays of Oil-Shale Drill Cores and Rotary Cuttings from the Greater Green River Basin, Southwestern Wyoming: U.S. Geological Survey Open-File Report 2008–1152. 2 chaps., 1 CD–ROM.

Arenas, C., Cabrera, L., Ramos, E., 2007. Sedimentology of tufa facies and continental microbialites from the palaeogene of Mallorca Island (Spain). Sediment. Geol. 197, 1–27.

Arenas-Abad, C., Vázquez-Urbez, M., Pardo-Tirapu, G., Sancho-Marcén, A., 2010. Chapter 3 fluvial and associated carbonate deposits. In: Alonso-Zarza, A.M., Tanner, L.H. (Eds.), Developments in Sedimentology. Elsevier, pp. 133–175.

Aswasereelert, W., Meyers, S., Carroll, A., Peters, S., Smith, M., Feigl, K., 2013. Basin-scale cyclostratigraphy of the Green River Formation, Wyoming. Bulletin 125, 216–228.

Awramik, S.M., Buchheim, H.P., 2015. Giant stromatolites of the Eocene Green River Formation (Colorado, USA). Geology 43, 691–694.

Baddouh, M., Meyers, S.R., Carroll, A.R., Beard, B.L., Johnson, C.M., 2016. Lacustrine 87Sr/86Sr as a tracer to reconstruct Milankovitch forcing of the Eocene hydrologic cycle. Earth Planet. Sci. Lett. 448, 62–68.

Baddouh, M., Carroll, A.R., Meyers, S.R., Beard, B.L., Johnson, C.M., 2017. Chronostratigraphic correlation of lacustrine deposits using 87SR/86SR ratios, Eocene Green River Formation, Wyoming, USA. J. Sediment. Res. 87, 406–423.

Banner, J.L., Hanson, G.N., 1990. Calculation of simultaneous isotopic and trace element variations during water-rock interaction with applications to carbonate diagenesis. Geochim. Cosmochim. Acta 54, 3123–3137.

Bataille, C.P., Bowen, G.J., 2012. Mapping $^{87}Sr/^{86}Sr$ variations in bedrock and water for large scale provenance studies. Chem. Geol. 304-305, 39–52.

Beard, B., Johnson, C., 2000. Strontium Isotope Composition of Skeletal Material Can Determine the Birth Place and Geographic Mobility of Humans and Animals.

Benson, L., 1994. Carbonate deposition, Pyramid Lake subbasin, Nevada: 1. Sequence of formation and elevational distribution of carbonate deposits (Tufas). Palaeogeogr. Palaeoclimatol. Palaeoecol. 109, 55–87.

Benson, L.V., 2004. The Tufas of Pyramid Lake, Nevada. US Geol. Surv. Circ. 1267, 14.

Benson, L., Peterman, Z., 1996. Carbonate deposition, Pyramid Lake subbasin, Nevada: 3. The use of 87Sr values in carbonate deposits (tufas) to determine the hydrologic state of paleolake systems. Palaeogeogr. Palaeoclimatol. Palaeoecol. 119, 201–213.

Benson, L.V., Burdett, J.W., Kashgarian, M., Lund, S.P., Phillips, F.M., Rye, R.O., 1996. Climatic and hydrologic oscillations in the Owens Lake Basin and Adjacent Sierra Nevada, California. Science 274, 746–749.

Bishop, J.W., Osleger, D.A., Montañez, I., Sumner, D.Y., 2014. Meteoric diagenesis and fluid-rock interaction in the Middle Permian Capitan backreef: Yates Formation, Slaughter Canyon, New Mexico Diagenesis, Capitan Backreef, Yates Formation, New Mexico. AAPG Bull. 98, 1495–1519.

Bohacs, K.M., Carroll, A.R., Neal, J.E., Mankiewicz, P.J., 2000. Lake-basin type, source potential, and hydrocarbon character: an integrated sequence-stratigraphic-geochemical framework. Lake basins through space and time. AAPG Stud. Geol. 46, 3–34.

Bradley, W.H., 1929. The Varves and Climate of the Green River Epoch. 158E. U. S. Geological Survey Professional Paper. pp. 87–110.

Capo, R.C., Stewart, B.W., Chadwick, O.A., 1998. Strontium isotopes as tracers of ecosystem processes: theory and methods. Geoderma 82 (1), 197–225.

Carroll, A.R., 2017. Xenoconformities and the stratigraphic record of paleoenvironmental change. Geology 45, 639–642.

Carroll, A.R., Bohacs, K.M., 1999. Stratigraphic classification of ancient lakes: balancing tectonic and climatic controls. Geology 27, 99–102.

Carroll, A.R., Chetel, L.M., Smith, M.E., 2006. Feast to famine: sediment supply control on Laramide basin fill. Geology 34, 197–200.

Carroll, A.R., Doebbert, A.C., Booth, A.L., Chamberlain, C.P., Rhodes-Carson, M.K., Smith, M.E., Johnson, C.M., Beard, B.L., 2008. Capture of high-altitude precipitation by a low-altitude Eocene lake, western U.S. Geology 36, 791–794.

Cohen, A.S., 2003. Palaeolimnology: The History and Evolution of Lake Systems. Oxford University Press, Oxford, UK.

Culbertson, W.C., 1961. Stratigraphy of the Wilkins Peak Member of the Green River Formation, Firehole Basin Quadrangle, Wyoming. US Geol. Surv. Prof. Pap. 424D, 170–173.

Davidson, S.K., Hartley, A.J., 2010. Towards a quantitative method for estimating paleohydrology from clast size and comparison with modern rivers. J. Sediment. Res. 80, 688–702.

Dickinson, W.R., Klute, M.A., Hayes, M.J., Janecke, S.U., Lundin, E.R., McKittrick, M.A., Olivares, M.D., 1988. Paleogeographic and paleotectonic setting of Laramide sedimentary basins in the central Rocky Mountain region. GSA Bull. 100, 1023–1039.

Doebbert, A.C., Carroll, A.R., Mulch, A., Chetel, L.M., Chamberlain, C.P., 2010. Geomorphic controls on lacustrine isotopic compositions: evidence from the Laney Member, Green River Formation, Wyoming. GSA Bull. 122, 236–252.

Doebbert, A.C., Johnson, C.M., Carroll, A.R., Beard, B.L., Pietras, J.T., Rhodes Carson, M., Norsted, B., Throckmorton, L.A., 2014. Controls on Sr isotopic evolution in lacustrine systems: Eocene Green River Formation, Wyoming. Chem. Geol. 380, 172–189.

Dunn, J.R., 1953. The origin of the deposits of tufa in Mono Lake [California]. J.

Sediment. Res. 23, 18–23.

Emdadi, A., Gikas, P., Farazaki, M., Emami, Y., 2016. Salinity gradient energy potential at the hyper saline Urmia Lake – ZarrinehRud River system in Iran. Renew. Energy 86, 154–162.

Eugster, H.P., Hardie, L.A., 1975. Sedimentation in an ancient playa-lake complex; the Wilkins Peak Member of the Green River Formation of Wyoming. Geol. Soc. Am. Bull. 86, 319–334.

Fan, M., Dettman, D.L., 2009. Late paleocene high laramide ranges in Northeast Wyoming: oxygen isotope study of ancient river water. Earth Planet. Sci. Lett. 286, 110–121.

Fan, Y.-X., Chen, F.-H., Wei, G.-X., Madsen, D.B., Oviatt, C.G., Zhao, H., Chun, X., Yang, L.-P., Fan, T.-L., Li, G.-Q., 2010. Potential water sources for late Quaternary Megalake Jilantai-Hetao, China, inferred from mollusk shell 87Sr/86Sr ratios. J. Paleolimnol. 43, 577–587.

Faure, G., Powell, J., 1972. Strontium isotope geology. In: Mineral, Rocks and Inorganic Materials: Monograph Series of Theoretical and Experimental Studies 5. Springer-Verlag, New York.

García del Cura, M.A., Sanz-Montero, M.E., de los Rios, M.A., Ascaso, C., 2014. Microbial dolomite in fresh water carbonate deposits. Sedimentology 61, 41–55.

Conrad D. Gebelein, Paul Hoffman, 1973, Algal Origin of Dolomite Laminations in Stromatolitic Limestone: SEPM Journal of Sedimentary Research, doi:10.1306/74d72815-2b21-11d7-8648000102c1865d.

Gelband, S.D., Edelman-Furstenberg, Y., Stein, M., Starinsky, A., 2019. Formation of lacustrine dolomite in the late miocene marginal lakes of the East Mediterranean (northern Israel). Sedimentology 66, 2950–2975.

Gierlowski-Kordesch, E., Jacobson, A., Blum, J., Valero Garcés, B.L., 2008. Watershed reconstruction of a Paleocene–Eocene lake basin using Sr isotopes in carbonate rocks. Geol. Soc. Am. Bull. 120, 85–95.

Hammond, A.P., Carroll, A.R., Smith, M.E., Lowenstein, T.K., 2019. Bicarbonate Rivers: connecting Eocene magmatism to the world's largest Na-carbonate evaporite. Geology 47, 1020–1024.

Hart, W.S., Quade, J., Madsen, D.B., Kaufman, D.S., Oviatt, C.G., 2004. The 87Sr/86Sr ratios of lacustrine carbonates and lake-level history of the Bonneville paleolake system. Geol. Soc. Am. Bull. 116, 1107–1119.

Horton, T.W., Defliese, W.F., Tripati, A.K., Oze, C., 2016. Evaporation induced 18O and 13C enrichment in lake systems: a global perspective on hydrologic balance effects. Quat. Sci. Rev. 131, 365–379.

Hudson, A.M., Quade, J., Ali, G., Boyle, D., Bassett, S., Huntington, K.W., De los Santos, M.G., 2017. Stable C, O and clumped isotope systematics and 14C geochronology of carbonates from the Quaternary Chewaucan closed-basin lake system, Great Basin, USA: Implications for paleoenvironmental reconstructions using carbonates. Geochim. Cosmochim. Acta 212, 274–302.

Jagniecki, E.A., Lowenstein, T.K., Demicco, R.V., Baddouh, M., Carroll, A.R., Beard, B.L., Johnson, C.M., 2016. Paleohydrology of spring deposits in the Wilkins Peak Member of the Eocene Green River Formation. Geological Society of America Abstracts with Programs, Bridger Basin, WY, pp. 48 No.7 (Denver, CO Sept 25-28).

Jellison, R., Anderson, R.F., Melack, J.M., Heil, D., 1996. Organic matter accumulation in sediments of hypersaline Mono Lake during a period of changing salinity. Limnol. Oceanogr. 41, 1539–1544.

Johnson, R.C., Mercier, T.J., Brownfield, M.E., 2011. Assessment of In-place Oil Shale Resources of the Green River Formation, Greater Green River Basin in Wyoming, Colorado, and Utah. U.S. Geological Survey Digital Data Series 0069-DD.

Kempe, S., Kazmierczak, J., Landmann, G., Konuk, T., Reimer, A., Lipp, A., 1991. Largest known microbialites discovered in Lake Van, Turkey. Nature 349, 605.

Leggitt, L. V., Biaggi, R.E., and Buchheim, P.H., 2007, Palaeoenvironments associated with caddisfly-dominated microbial-carbonate mounds from the Tipton Shale Member of the Green River Formation: Eocene Lake Gosiute: Sedimentology, doi:10.1111/j.1365-3091.2007.00854.x.

Leggitt, V.L., Cushman Jr., R.A., 2001. Complex caddisfly-dominated bioherms from the Eocene Green River Formation. Sediment. Geol. 145, 377–396.

Leggitt, V.L., Loewen, M.A., 2002. Eocene Green River Formation "Oocardium tufa" reinterpreted as complex arrays of calcified caddisfly (Insecta: Trichoptera) larval cases. Sediment. Geol. 148, 139–146.

Li, H.-C., Ku, T.-L., 1997. δ13C–δ18O covariance as a paleohydrological indicator for closed-basin lakes. Palaeogeogr. Palaeoclimatol. Palaeoecol. 133, 69–80.

Lohmann, K.C., 1988. Geochemical Patterns of Meteoric Diagenetic Systems and Their Application to Studies of Paleokarst, Paleokarst. Springer, pp. 58–80.

Love, J.D., Christiansen, A.C., 1985. Geologic Map of Wyoming. US Geological Suervey.

Lowenstein, T.K., Jagniecki, E.A., Carroll, A.R., Smith, M.E., Renaut, R.W., Owen, R.B., 2017. The Green River salt mystery: what was the source of the hyperalkaline lake waters? Earth Sci. Rev. 173, 295–306.

Machlus, M.L., Ramezani, J., Bowring, S.A., Hemming, S.R., Tsukui, K., Clyde, W.C., 2015. A strategy for cross-calibrating U–Pb chronology and astrochronology of sedimentary sequences: an example from the Green River Formation, Wyoming, USA. Earth Planet. Sci. Lett. 413, 70–78.

Mason, Glenn M., 2012. Stratigraphic distribution and mineralogic correlation of the

Green River Formation, Green River and Washakie Basins, Wyoming, U.S.a. In: Baganz, O.W., Bartov, Y., Bohacs, K., Nummedal, D. (Eds.), Lacustrine Sandstone Reservoirs and Hydrocarbon Systems. AAPG Memoir, vol. 95. pp. 223–253.

McKenzie, J., 1985. Carbon isotopes and productivity in the lacustrine and marine environment. Chem. Process. Lakes 99–118.

Neumann, K., Dreiss, S., 1995. Strontium 87/strontium 86 ratios as tracers in groundwater and surface waters in Mono Basin, California. Water Resour. Res. 31, 3183–3193.

Pedone, V.A., Dickson, J.A.D., 2000. Replacement of aragonite by quasi-rhombohedral dolomite in a late Pleistocene tufa mound, Great Salt Lake, Utah, U.S.a. J. Sediment. Res. 70, 1152–1159.

Pietras, J.T., 2003. High-Resolution Sequence Stratigraphy and Strontium Isotope Geochemistry of the Lacustrine Wilkins Peak Member, Eocene Green River Formation, Wyoming. United States of America. University of Wisconsin-Madison, pp. 372 Ph.D. dissertation.

Pietras, J.T., Carroll, A.R., 2006. High-resolution stratigraphy of an underfilled lake basin: Wilkins Peak member, Eocene Green River Formation, Wyoming, USA. J. Sediment. Res. 76, 1197–1214.

Renaut, R.W., Owen, R.B., Lowenstein, T.K., de Cort, G., Mcnulty, E., Scott, J.J., Mbuthia, A., 2020. The role of hydrothermal fluids in sedimentation in saline alkaline lakes: evidence from Nasikie Engida, Kenya Rift Valley. Sedimentology. https://doi.org/10.1111/sed.12778. Accepted Author Manuscript.

Rhodes, M.K., Carroll, A.R., Pietras, J.T., Beard, B.L., Johnson, C.M., 2002. Strontium isotope record of paleohydrology and continental weathering, Eocene Green River Formation, Wyoming. Geology 30, 167–170.

Roehler, H.W., 1989. Correlation of Surface Sections of the Intertongued Eocene Wasatch and Green River Formations along the Western Margins of the Greater Green River Basin in Southwest Wyoming. Miscellaneous Field Studies Map ed.

Roehler, H.W., 1992. Correlation, Composition, Areal Distribution, and Thickness of Eocene Stratigraphic Units, Greater Green River Basin, Wyoming, Utah, and Colorado. U.S. Geological Survey, pp. 49 Professional Paper 1506-E.

Roehler, H.W., 1993. Eocene Climates, Depositional Environments, and Geography, Greater Green River Basin, Wyoming, Utah, and Colorado. United States Geological Survey Professional Paper.

Rhodes, M.K., and Carroll, A.R., 2015, Lake Type Transition from Balanced-Fill to Overfilled: Laney Member, Green River Formation, Washakie Basin, Wyoming, doi:10.1007/978-94-017-9906-5_5.

Seard, C., Camoin, G., Rouchy, J.-M., Virgone, A., 2013. Composition, structure and evolution of a lacustrine carbonate margin dominated by microbialites: case study from the Green River formation (Eocene; Wyoming, USA). Palaeogeogr. Palaeoclimatol. Palaeoecol. 381, 128–144.

Smith, G.I., 2009. Late Cenozoic geology and lacustrine history of Searles Valley, Inyo and San Bernardino Counties, California. U.S. Geological Survey, pp. 115 Professional Paper 1727. 4 plates.

Smith, M.E., Singer, B., Carroll, A., 2003. 40Ar/39Ar geochronology of the Eocene Green River Formation, Wyoming. Geol. Soc. Am. Bull. 115, 549–565.

Smith, M.E., Singer, B.S., Carroll, A.R., Fournelle, J.H., 2006. High-resolution calibration of Eocene strata: 40Ar/39Ar geochronology of biotite in the Green River Formation. Geology 34, 393–396.

Smith, M.E., Carroll, A.R., Singer, B.S., 2008. Synoptic reconstruction of a major ancient lake system: Eocene Green River Formation, western United States. GSA Bull. 120, 54–84.

Smith, M.E., Chamberlain, K., Singer, B., Carroll, A., 2010. Eocene clocks agree: Coeval 40Ar/39Ar, U-Pb, and astronomical ages from the Green River Formation. Geology 38, 527–530.

Smith, M.E., Carroll, A.R., Scott, J.J., Singer, B.S., 2014. Early Eocene carbon isotope excursions and landscape destabilization at eccentricity minima: Green River Formation of Wyoming. Earth Planet. Sci. Lett. 403, 393–406.

Smith, M.E., Carroll, A.R., Scott, J.J., 2015. Stratigraphic expression of climate, tectonism, and geomorphic forcing in an underfilled lake basin: Wilkins Peak Member of the Green River Formation, Stratigraphy and Paleolimnology of the Green River Formation, Western USA. Springer, pp. 61–102.

Smoot, J.P., 1983. Depositional subenvironments in an arid closed basin; the Wilkins Peak Member of the Green River Formation (Eocene), Wyoming, USA. Sedimentology 30, 801–827.

Talbot, M., 1990. A review of the palaeohydrological interpretation of carbon and oxygen isotopic ratios in primary lacustrine carbonates. Chem. Geol. Isot. Geosci. Sect. 80, 261–279.

Törö, B., Pratt, B.R., 2015. Eocene paleoseismic record of the Green River Formation, Fossil Basin, Wyoming, U.S.A.: implications of synsedimentary deformation structures in lacustrine carbonate mudstones. J. Sediment. Res. 85, 855–884.

Trampush, S., Huzurbazar, S., McElroy, B., 2014. Empirical assessment of theory for bankfull characteristics of alluvial channels. Water Resour. Res. 50, 9211–9220.

Wolfbauer, C.A., Surdam, R.C., 1974. Origin of nonmarine dolomite in eocene lake Gosiute, Green River Basin, Wyoming. Geol. Soc. Am. Bull. 85, 1733–1740.